Chemistry of *C*-Trimethylsilyl-Substituted Heterocarboranes. 12. Synthetic, Structural, and Bonding Studies on the "Carbons Apart" *closo*- and *commo*-Nickelacarboranes Derived from "Carbons Adjacent" *closo*-Carborane 1,2-$(SiMe_3)_2$-1,2-$C_2B_4H_4$†

Hongming Zhang, Ying Wang, Anil K. Saxena, Aderemi R. Oki, John A. Maguire, and Narayan S. Hosmane*

Department of Chemistry, Southern Methodist University, Dallas, Texas 75275

Received April 20, 1993®

The reaction of "carbons adjacent" *closo*-1,2-$(SiMe_3)_2$-1,2-$C_2B_4H_4$ with lithium naphthalide in THF produces the "carbons apart" dilithium compound *closo-exo*-5,6-[$(\mu$-H)$_2$Li(THF)](μ-THF)-1-Li-2,4-$(SiMe_3)_2$-2,4-$C_2B_4H_4$ (**I**), that exists as discrete dimers in the solid state. However, when the reaction was carried out in TMEDA, the monomeric carbons apart dilithiacarborane *closo-exo*-5,6-[$(\mu$-H)$_2$Li(TMEDA)]-1-Li(TMEDA)-2,4-$(SiMe_3)_2$-2,4-$C_2B_4H_4$ (**II**) was isolated in 90% yield. The ^{1}H, ^{7}Li, ^{11}B, and ^{13}C NMR spectra and IR spectra of **I** and **II** are all consistent with their molecular formulas. The reaction of the THF-solvated dilithium compound, **I**, with anhydrous $NiCl_2$ in a 1:1 molar ratio, in a 1:1 mixture of *n*-hexane and THF, produced the carbons apart nickel sandwich *commo*-1,1′-Ni[2,4-$(SiMe_3)_2$-2,4-$C_2B_4H_4$]$_2$ (**III**), along with elemental nickel (Ni^0). On the other hand, a TMEDA-complexed species, *closo*-1-Ni(TMEDA)-2,4-$(SiMe_3)_2$-2,4-$C_2B_4H_4$ (**IV**), was isolated from the analogous reaction of $NiCl_2$ with the TMEDA-solvated dilithium compound, **II**. The nickelacarboranes were also characterized by ^{1}H, ^{11}B, and ^{13}C NMR spectra, IR and mass spectra, and elemental analyses. The molecular structures of **I**–**IV** were determined by X-ray diffraction. The *closo*-nickelacarborane (**IV**), a formal Ni(II) half-sandwich, was also produced in a redox reaction involving *commo*-Ni(IV) sandwich **III** in wet TMEDA at room temperature. While the *closo*-dilithium compounds, **I** and **II**, crystallized in the monoclinic space group $P2_1/n$, the *commo*-nickelacarborane (**III**) and *closo*-nickelacarborane (**IV**) crystallized in orthorhombic and monoclinic space groups *Pbcn* and $P2_1/n$, respectively, with a = 11.353(5), 9.828(4), 12.409(3), and 8.310 (2) Å, b = 17.490(7), 22.267(7), 18.436(5), and 19.657(4) Å, c = 13.273(6), 15.064(5), 12.976(3), and 14.655(3) Å, β = 104.33(3), 95.87(3), 90.00, and 94.14(2)°, V = 2551(2), 3279(2), 2969(1), and 2387.6(9) Å^3, and Z = 2, 4, 4, and 4. The final refinements of **I**–**IV** converged at R = 0.076, 0.060, 0.033, and 0.041 and R_w = 0.095, 0.064, 0.040, and 0.052, respectively.

Introduction

Recently, we have shown that the reactions of the dilithium-complexed "carbons adjacent" *nido*-carborane dianions [2-$(SiMe_3)$-3-(R)-2,3-$C_2B_4H_4]^{2-}$ (R = $SiMe_3$, Me) with anhydrous $NiCl_2$ in *n*-hexane, THF, or TMEDA produced the corresponding *closo*-1,2-dicarbahexaborane-(6) derivatives in 40–59% yields.[1] Prior to these results the most direct route to the *closo*-carboranes involved the initial preparation of *closo*-stannacarborane precursors, followed by their oxidative cage closure using expensive platinum reagents, such as $PtCl_2$ or $PtCl_4$.[2] Since these *closo*-C_2B_4-carborane cages can be reductively opened to generate the corresponding "carbons apart" *nido*-carborane dianions[3] that were subsequently utilized as synthons for a variety of metallacarboranes,[4] the new synthetic route was considered as an important development in the chemistry of metallacarboranes. The extent to which these new dianions can function as ligands depends on their stability toward oxidation. Therefore, a central question is what type of reaction would take place between the group 1 complexed carbons apart dianion and a salt such as $NiCl_2$. Would the reaction be a redox process leading to a *closo*-carborane or would it result in the formation of a nickelacarborane? If oxidative cage closure takes place, will the product be the corresponding carbons apart *closo*-1-$(SiMe_3)$-6-(R)-1,6-$C_2B_4H_4$ derivative or will the original precursor, *closo*-1-$(SiMe_3)$-2-(R)-1,2-$C_2B_4H_4$, be reformed? If metallacarboranes are formed, it would be of interest to investigate their stoichiometries and structures. Therefore, as part of our investigation of the reaction chemistry of the carbons apart carboranes, we have studied the reactivity of their THF- and TMEDA-solvated *closo*-dilithiacarboranes toward $NiCl_2$. Here, we report the details of these reactions, spectroscopic characterization, and the crystal structures of the carbons apart dilithium

† Dedicated to Professor John J. Banewicz on the occasion of his retirement from active teaching and research at Southern Methodist University.

® Abstract published in *Advance ACS Abstracts*, September 1, 1993.

(1) Hosmane, N. S.; Saxena, A. K.; Barreto, R. D.; Zhang, H.; Maguire, J. A.; Jia, L.; Wang, Y.; Oki, A. R.; Grover, K. V.; Whitten, S. J.; Dawson, K.; Tolle, M. A.; Siriwardane, U.; Demissie, T.; Fagner, J. S. *Organometallics* **1993**, *12*, 3001.

(2) Hosmane, N. S.; Barreto, R. D.; Tolle, M. A.; Alexander, J. J.; Quintana, W.; Siriwardane, U.; Shore, S. G.; Williams, R. E. *Inorg. Chem.* **1990**, *29*, 2698.

(3) (a) Hosmane, N. S.; Jia, L.; Zhang, H.; Bausch, J. W.; Prakash, G. K. S.; Williams, R. E.; Onak, T. P. *Inorg. Chem.* **1991**, *30*, 3793. (b) Bausch, J. W. Ph.D. Thesis, University of Southern California, 1991.

(4) Jia, L.; Wang, Y.; Saxena, A. K.; Oki, A. R.; Zhang, H.; Maguire, J. A.; Hosmane, N. S. Paper presented at the BUSA-III meeting, Pullman, WA, July, 1992; Jia, L. M.S. Thesis, Southern Methodist University, 1992.

0276-7333/93/2312-3933$04.00/0

compounds *closo-exo*-5,6-[$(\mu$-H)$_2$Li(THF)](μ-THF)-1-Li-2,4-(SiMe$_3$)$_2$-2,4-$C_2B_4H_4$ (**I**) and *closo-exo*-5,6-[$(\mu$-H)$_2$Li(TMEDA)]-1-Li(TMEDA)-2,4-(SiMe$_3$)$_2$-2,4-$C_2B_4H_4$ (**II**) and the carbons apart nickelacarborane products *commo*-1,1′-Ni[2,4-(SiMe$_3$)$_2$-2,4-$C_2B_4H_4$]$_2$ (**III**) and *closo*-1-Ni(TMEDA)-2,4-(SiMe$_3$)$_2$-2,4-$C_2B_4H_4$ (**IV**).

Experimental Section

Materials. 1,2-Bis(trimethylsilyl)-1,2-dicarba-*closo*-hexaborane(6) was prepared by the method described by Hosmane *et al.*[1,2] Prior to use, *N,N,N,N*-tetramethylethylenediamine, TMEDA (Aldrich), was distilled *in vacuo* and stored over sodium metal. The purity was checked by IR and NMR spectra and boiling point measurements. Before use, naphthalene (Aldrich) was sublimed *in vacuo*, Li metal (Aldrich) was freshly cut in a drybox, and $NiCl_2$ (Aldrich) was dried *in vacuo* by heating at 120 °C overnight. Benzene, tetrahydrofuran (THF), and *n*-hexane were dried over $LiAlH_4$ and doubly distilled; all other solvents were dried over 4–8-mesh molecular sieves (Aldrich) and either saturated with dry argon or degassed before use.

Spectroscopic and Analytical Procedures. Proton, lithium-7, boron-11, and carbon-13 pulse Fourier transform NMR spectra, at 200, 77.7, 64.2, and 50.3 MHz, respectively, were recorded on an IBM-WP200 SY multinuclear NMR spectrometer. Infrared spectra were recorded on a Perkin-Elmer Model 283 infrared spectrophotometer and a Perkin-Elmer Model 1600 FT-IR spectrophotometer. High resolution electron impact (HREI) mass spectral determinations were performed at the Midwest Center for Mass Spectrometry, University of Nebraska—Lincoln, Nebraska. Elemental analyses were obtained from Oneida Research Services (ORS) Inc., Whitesboro, NY.

Synthetic Procedures. All experiments were carried out in Pyrex glass round bottom flasks of 250-mL capacity, containing magnetic stirring bars and fitted with high-vacuum Teflon valves. Nonvolatile substances were manipulated in either a drybox or evacuable glovebags under an atmosphere of dry nitrogen. All known compounds among the products were identified by comparing their IR and NMR spectra with those of the authentic samples.

Synthesis of Dimeric *closo-exo*-5,6-[$(\mu$-H)$_2$Li(C_4H_8O)](μ-C_4H_8O)-1-Li-2,4-(SiMe$_3$)$_2$-2,4-$C_2B_4H_4$ (I). In a procedure identical with that employed in the syntheses of carbons apart dianions of C_2B_4-carboranes,[3] 0.74 mmol (0.16 g) of *closo*-1,2-(SiMe$_3$)$_2$-1,2-$C_2B_4H_4$ in tetrahydrofuran (THF) was allowed to react for several minutes with 1.58 mmol of lithium naphthalide, prepared from freshly cut Li metal (0.011 g) and $C_{10}H_8$ (0.21 g), in THF (10–15 mL) at room temperature, during which time the heterogeneous mixture turned dark-brown. The ^{11}B NMR spectrum of this mixture indicated that the *closo*-carborane was completely consumed in the reaction. At this point, the dark-brown solution in the flask was filtered *in vacuo* and all the volatiles, including naphthalene, were removed from the filtrate at 40 °C, leaving behind a yellow-brown solid, which was later identified as *closo-exo*-5,6-[$(\mu$-H)$_2$Li(C_4H_8O)](μ-C_4H_8O)-1-Li-2,4-(SiMe$_3$)$_2$-2,4-$C_2B_4H_4$ (**I**) (0.252 g, 0.68 mmol; 93% yield; mp 147–148 °C dec; soluble in THF, C_6H_6, $CDCl_3$, CH_2Cl_2, and CD_3CN and sparingly soluble in *n*-hexane). This solid was washed with dry *n*-hexane and dried *in vacuo* and then recrystallized from benzene solution to give transparent prismatic crystals whose X-ray analysis (discussed below) showed it to be a dimeric form of **I**. Since **I** is extremely sensitive to air and/or moisture, reproducible microanalytical data could not be obtained, even for single-crystal samples. The spectroscopic data for **I**: ^{1}H NMR (THF-d_8, relative to external Me_4Si) δ 3.56 [s (br), 8H, THF], 1.71 [s (br), 8H, THF], −0.05 [s, 18H, $SiMe_3$], the BH resonances are masked by those of THF's; ^{7}Li NMR (THF-d_8, relative to external aqueous $LiNO_3$) δ 2.73 [s (v br), *endo*-cage Li], 1.42 [s (br), *exo*-cage Li]; ^{11}B NMR (THF-d_8, relative to external BF_3·OEt_2) δ 16.25 [br, ill-defined peak, 1B, basal BH], 13.94 [d (br), 2B, basal BH, $^1J(^{11}B-^1H)$ = unresolved], −42.28 [d (br), 1B, apical BH, $^1J(^{11}B-^1H)$ = 154.7 Hz]; ^{13}C NMR (THF-d_8, relative to external Me_4Si) δ 85.27 [s (br), cage carbons (SiCB)], 67.92 [br, ill-defined peak, THF], 25.27 [br, ill-defined peak, THF], −0.25 [q, $SiMe_3$, $^1J(^{13}C-^1H)$ = 116.08 Hz]; IR [cm^{-1}, THF-d_8 vs THF-d_8] 2999 (sh), 2913 (s, s), 2841 (sh) [ν(C–H)], 2681 (w, s), 2370 (w, br), 2274 (w, br) [ν(B–H)], 2149 (w, s), 1973 (w, br) [B–H–Li (bridge)], 1447 (m, s) [δ(C–H) asym], 1368 (w, s), 1279 (w, s) [δ(C–H) sym], 1181 (w, br), 1070 (sh), 1050 (s, s), 910 (vvs, br), 851 (sh) [ρ(C–H)], 656 (w, br).

Synthesis of Monomeric *closo-exo*-5,6-[$(\mu$-H)$_2$Li(Me_2NCH_2)$_2$]-2,4-(SiMe$_3$)$_2$-2,4-$C_2B_4H_4$ (II). A TMEDA solution (5 mL) of *closo*-1,2-(SiMe$_3$)$_2$-1,2-$C_2B_4H_4$ (1.10 g, 5.05 mmol) was transferred *in vacuo* into a reaction flask containing 10.09 mmol of lithium naphthalide (prepared from 0.071 g of freshly cut Li metal and 1.293 g of $C_{10}H_8$) in 10 mL of TMEDA at −196 °C. The mixture in the flask was then warmed to room temperature and stirred constantly overnight, during which time the color of the solution turned dark-brown. At that point, the dark-brown solution in the flask was filtered *in vacuo* and all the volatiles, including naphthalene, were removed from the filtrate at 40 °C, leaving behind a yellow-brown solid, which was later identified as *closo-exo*-5,6-[$(\mu$-H)$_2$Li(Me_2NCH_2)$_2$]-1-Li[(Me_2NCH_2)$_2$]-2,4-(SiMe$_3$)$_2$-2,4-$C_2B_4H_4$ (**II**) (2.10 g, 4.54 mmol; 90% yield; mp 110 °C dec; soluble in THF, C_6H_6, $CDCl_3$, CH_2Cl_2, and CD_3CN and sparingly soluble in *n*-hexane). This solid was washed with dry *n*-hexane, dried *in vacuo*, and then recrystallized from benzene solution to give transparent platelike crystals of **II**. Since **II** is extremely sensitive to air and/or moisture, reproducible microanalytical data could not be obtained, even for single-crystal samples. The spectroscopic data for **II**: ^{1}H NMR (C_6D_6, relative to external Me_4Si) δ 2.41 [s (br), 4H, CH_2, TMEDA], 2.33 [s (br), 12H, Me, TMEDA], −0.46 [s, 9H, $SiMe_3$], the BH resonances are masked by those of TMEDA's; ^{7}Li NMR (C_6D_6, relative to external aqueous $LiNO_3$) δ −2.13 [s (br), *exo*-cage Li], −6.88 [s (v br), *endo*-cage Li]; ^{11}B NMR (C_6D_6, relative to external BF_3·OEt_2) δ 18.02 [br, ill-defined peak, 1B, basal BH], 6.56 [d (br), 2B, basal BH, $^1J(^{11}B-^1H)$ = unresolved], −48.78 (d (br), 1B, apical BH, $^1J(^{11}B-^1H)$ = 140.6 Hz]; ^{13}C NMR (C_6D_6, relative to external Me_4Si) δ 86.16 [s (br), cage carbons (SiCB)], 57.62 [t, 2C, CH_2, TMEDA, $^1J(^{13}C-^1H)$ = 132.3 Hz], 46.0 [q, 4C, Me, TMEDA, $^1J(^{13}C-^1H)$ = 133.1 Hz], 2.90 [q, 3C, $SiMe_3$, $^1J(^{13}C-^1H)$ = 117.24 Hz]; IR [cm^{-1}, C_6D_6 vs C_6D_6] 3233 (w, s), 2954 (s, s), 2900 (sh), 2850 (sh) [ν(C–H)], 2486 (m, br), 2387 (m, s), 2277 (vs, s) [ν(B–H)], 1860 (v w) [B–H–Li (bridge)], 1684 (w, s), 1617 (s, s), 1458 (m, br) [δ(C–H) asym], 1328 (m, s), 1240 (m, br) [δ(C–H) sym], 1186 (w, s), 1158 (w, s), 1030 (w, br), 944 (w, s), 841 (vvs, br) [ρ(C–H)], 677 (w, br), 522 (s, br).

Synthesis of *commo*-1,1′-Ni[2,4-(SiMe$_3$)$_2$-2,4-$C_2B_4H_4$]$_2$ (III). A 14.73-mmol (5.40-g) sample of *closo-exo*-5,6-[$(\mu$-H)$_2$Li(C_4H_8O)]-(μ-C_4H_8O)-1-Li-2,4-(SiMe$_3$)$_2$-2,4-$C_2B_4H_4$ (**I**) was dissolved *in vacuo* in 20 mL of a 1:1 mixture of *n*-hexane and THF at room temperature. The resulting clear solution was slowly poured *in vacuo* onto anhydrous $NiCl_2$ (1.91 g, 14.74 mmol) at 0 °C, and the resulting heterogeneous mixture was stirred at this temperature for 5 h and then at room temperature for 3 h, during which time the solution turned dark-brown with the formation of some black precipitate. After removal of *n*-hexane and THF at room temperature *in vacuo*, the reaction flask was attached to a series of detachable U-traps. Upon vacuum sublimation of the dark-brown residue at 120 °C, 1.35 g of a yellow crystalline solid, identified as *commo*-1,1′-Ni[2,4-(SiMe$_3$)$_2$-2,4-$C_2B_4H_4$]$_2$ (**III**) (2.73 mmol, 37% yield; mp 114–116 °C; soluble in both polar and nonpolar organic solvents), was collected in a detachable U-trap held at 0 °C. The side arms of both the reaction flask and the U-trap were maintained at 115–120 °C with heating tape during the sublimation. The gray-black residue that remained in the reaction flask after isolating **III** was dissolved in a water/acetone mixture, and the resulting turbid solution was filtered to collect a pale brown filtrate. After removal of all the solvents from the filtrate, a slightly colored solid was obtained (not measured) that was identified as LiCl by qualitative analysis and by comparing its ^{7}Li NMR spectrum with that of the authentic sample. The

gray solid (0.45 g), that remained on the frit, was identified by qualitative analysis as elemental nickel (Ni^0). Anal. Calcd for $C_{16}H_{44}B_8Si_4Ni$ (**III**): C, 38.93; H, 8.92. Found: C, 38.92; H, 8.94. The spectroscopic data for **III**: ^1H NMR (C_6D_6, relative to external Me_4Si) δ 5.1 [v br, ill-defined peak, 3H, basal H_t], 3.51 [q (br), 1H, apical H_t, $^1J(^1H-^{11}B)$ = 162 Hz], 0.42 [s (br), 9 H, $SiMe_3$], 0.33 [s, 9H, $SiMe_3$]; ^{11}B NMR (C_6D_6, relative to external $BF_3{\cdot}OEt_2$) δ 18.70 [v br, 3B, basal BH, $^1J(^{11}B-^1H)$ = unresolved], 5.92 [d, 1B, apical BH, $^1J(^{11}B-^1H)$ = 161.5 Hz]; ^{13}C NMR (C_6D_6, relative to external Me_4Si) δ 83.52 [s (br), cage carbons (SiCB)], 80.46 [s (br), cage carbons (SiCB)], 0.59 [q, 3C, $SiMe_3$, $^1J(^{13}C-^1H)$ = 119.11 Hz], 0.25 [q, 3C, $SiMe_3$, $^1J(^{13}C-^1H)$ = 119.22 Hz]; IR [cm^{-1}, C_6D_6 vs C_6D_6] 3430 (w, br), 3340 (w, s), 2940 (s, s), 2890 (s, br), 2850 (s, s) [ν(C-H)], 2550 (s, br) [ν(B-H)], 1340 (w, br) [δ(C-H) asym], 1250 (s, br), 1240 (sh) [δ(C-H) sym], 1150 (m, s), 1115 (w, s), 1040 (w, br), 980 (w, br), 890 (w, br), 835 (vvs, br) [ρ(C-H)], 750 (w, s), 680 (w, br), 620 (w, br), 470 (m, br). Mass spectral analysis (HREI): theoretical mass for the parent ion grouping of **III**, $[^{12}C_{16}{}^1H_{44}{}^{11}B_6{}^{10}B_2{}^{28}Si_4{}^{58}Ni]^+$, $[^{12}C_{16}{}^1H_{44}{}^{11}B_7{}^{10}B_1{}^{28}Si_4{}^{58}Ni]^+$, $[^{12}C_{16}{}^1H_{44}{}^{11}B_8{}^{28}Si_4{}^{58}Ni]^+$, $[^{12}C_{16}{}^1H_{44}{}^{11}B_7{}^{10}B_1{}^{28}Si_4{}^{60}Ni]^+$, $[^{12}C_{16}{}^1H_{44}{}^{11}B_8{}^{28}Si_4{}^{60}Ni]^+$, $[^{12}C_{15}{}^{13}C_1{}^1H_{44}{}^{11}B_8{}^{28}Si_4{}^{60}Ni]^+$, *m/z* 492.2690, 493.2654, 494.2618, 495.2633, 496.2597, and 497.2631; measured mass *m/z* 492.2689, 493,2653, 494.2639, 495,2619, 496.2595, and 497.2588, respectively.

Synthesis of *closo*-1-Ni[$(Me_2NCH_2)_2$]-2,4-$(SiMe_3)_2$-2,4-$C_2B_4H_4$ (IV). In a procedure identical with that described above for **III**, 5.05 mmol of *closo-exo*-5,6-[$(\mu$-H)$_2$Li$(Me_2NCH_2)_2$]-1-Li[$(Me_2NCH_2)_2$]-2,4-$(SiMe_3)_2$-2,4-$C_2B_4H_4$ (**II**) (2.343 g) was allowed to react with anhydrous $NiCl_2$ (0.656 g, 5.06 mmol) in dry benzene (30 mL) at 0 °C for 2 h with constant stirring and then at room temperature overnight, during which time the solution turned dark-brown. After removal of solvent, benzene, and the uncoordinated TMEDA (not measured) at room temperature *in vacuo*, the reaction flask was attached to a series of detachable U-traps. Upon vacuum sublimation of the dark-brown residue at 120 °C, 0.05 g of a yellow crystalline solid, identified as *commo*-1,1′-Ni[2,4-$(SiMe_3)_2$-2,4-$C_2B_4H_4]_2$ (**III**) (0.10 mmol, 4% yield) was collected in a detachable U-trap held at 0 °C. After complete removal of **III**, the reaction flask was attached to another detachable U-trap that was maintained at 0 °C. A further vacuum sublimation of the dark residue at 155 °C, yielded 1.17 g of a dark-red solid which was later identified as the *closo*-nickelacarborane 1-Ni[$(Me_2NCH_2)_2$]-2,4-$(SiMe_3)_2$-2,4-$C_2B_4H_4$ (**IV**) (collected at 0 °C; 2.98 mmol, 59% yield; mp 158–160 °C; soluble in benzene, TMEDA, THF, and other polar organic solvents but slightly soluble in *n*-hexane). The side arms of both the reaction flask and the U-trap were maintained at 150–155 °C with heating tape during the sublimation. The final gray-black residue, that remained in the reaction flask after complete removal of **IV**, was identifed as a mixture of LiCl and elemental nickel (Ni^0), as described above. Anal. Calcd for $C_{14}H_{38}N_2B_4Si_2Ni$ (**IV**): C, 42.83; H, 9.76; N, 7.14. Found: C, 41.07; H, 9.00; N, 7.33. The spectroscopic data for **IV**: ^1H NMR (C_6D_6, relative to external Me_4Si) δ 4.51 [q (br, overlapping), 2H, basal H_t], 3.42 [q (br, overlapping), 1H, basal H_t], 2.17 [q (br), 1H, apical H_t, $^1J(^1H-^{11}B)$ = 154 Hz], 2.05 [s (br), 4H, CH_2, TMEDA], 1.95 [s (br), 12H, Me, TMEDA], 0.56 [s (br), 18H, $SiMe_3$]; ^{11}B NMR (C_6D_6, relative to external $BF_3{\cdot}OEt_2$) δ 3.72 [v br, 2B, basal BH, $^1J(^{11}B-^1H)$ = unresolved], -3.74 (v br, 1B, basal BH, $^1J(^{11}B-^1H)$ = unresolved], -10.81 [d,1B, apical BH, $^1J(^{11}B-^1H)$ = 154.4 Hz]; ^{13}C NMR (C_6D_6, relative to external Me_4Si) δ 82.9 [s (br), cage carbons (SiCB)], 60.2 [t, 1C, CH_2, TMEDA, $^1J(^{13}C-^1H)$ = 137.5 Hz], 59.1 [t, 1C, CH_2, TMEDA, $^1J(^{13}C-^1H)$ = 136.5 Hz], 53.4 [q, 2C, Me, TMEDA, $^1J(^{13}C-^1H)$ = 138.5 Hz], 52.8 [q, 2C, Me, TMEDA, $^1J(^{13}C-^1H)$ = 138.9 Hz], 2.1 [q, 6C, $SiMe_3$, $^1J(^{13}C-^1H)$ = 118.5 Hz]; IR [cm^{-1}, C_6D_6 vs C_6D_6] 3432 (w, br), 3092 (w, br), 2952 (w, s), 2888 (w, s), 2876 (w, s) [ν(C-H)], 2488 (s, s), 2323 (w, s) [ν(B-H)], 1959 (s, s), 1816 (s, s), 1752 (w, s), 1478 (s, br) [δ(C-H) asym], 1240 (m, br) [δ(C-H) asym], 1188 (m, br), 1036 (m, s), 840 (vs, br) [ρ-(C-H)], 671 (s, br), 560 (m, br). Mass spectral analysis (HREI): theoretical mass for the parent ion grouping of **IV**, $[^{12}C_{14}{}^1H_{38}{}^{14}N_2{}^{11}B_2{}^{10}B_2{}^{28}Si_2{}^{58}Ni]^+$, $[^{12}C_{14}{}^1H_{38}{}^{14}N_2{}^{11}B_3{}^{10}B_1{}^{28}Si_2{}^{58}Ni]^+$, $[^{12}C_{14}{}^1H_{38}{}^{14}N_2{}^{11}B_4{}^{28}Si_2{}^{58}Ni]^+$, $[^{12}C_{14}{}^1H_{38}{}^{14}N_2{}^{11}B_3{}^{10}B_1{}^{28}Si_2{}^{60}Ni]^+$, $[^{12}C_{14}{}^1H_{38}{}^{14}N_2{}^{11}B_4{}^{28}Si_2{}^{60}Ni]^+$, $[^{12}C_{13}{}^{13}C_1{}^1H_{38}{}^{14}N_2{}^{11}B_4{}^{28}Si_2{}^{60}Ni]^+$, *m/z* 390.2372, 391.2335, 392.2299, 393.2314, 394.2278, and 395.2311; measured mass *m/z* 390.2365, 391.2335, 392.2309, 393.2298, 394.2274, and 395.2300, respectively.

Conversion of *commo*-1,1′-Ni[2,4-$(SiMe_3)_2$-2,4-$C_2B_4H_4]_2$ (III) to *closo*-1-Ni[$(Me_2NCH_2)_2$]-2,4-$(SiMe_3)_2$-2,4-$C_2B_4H_4$ (IV). A 0.42-mmol sample of *commo*-nickelacarborane **III** (0.21 g) was dissolved in 5 mL of reagent-grade (undried) TMEDA, and the resulting greenish yellow solution was stirred at room temperature for 8 h, during which time the solution turned reddish brown. At this point, all the volatiles were transferred to the vacuum line at 40 °C and were fractionated through a series of traps held at -23 and -196 °C, which collected most of the unreacted TMEDA and the *closo*-carborane precursor 1,2-$(SiMe_3)_2$-1,2-$C_2B_4H_4$ (0.10 g, 0.46 mmol), respectively. The reddish brown solid residue in the flask was then sublimed *in vacuo*, as described above, to collect 0.14 g of the TMEDA-coordinated *closo*-nickelacarborane **IV** (0.36 mmol, 86% yield) in a detachable U-trap held at 0 °C. A very small quantity of the black residue, obtained after sublimation, was found to be insoluble in most of the organic solvents and was discarded without identification.

Crystal Structure Analyses of *closo-exo*-5,6-[$(\mu$-H)$_2$Li(THF)]$(\mu$-THF)-1-Li-2,4-$(SiMe_3)_2$-2,4-$C_2B_4H_4$ (I), *closo-exo*-5,6-[$(\mu$-H)$_2$Li(TMEDA)]-1-Li(TMEDA)-2,4-$(SiMe_3)_2$-2,4-$C_2B_4H_4$ (II), *commo*-1,1′-Ni[2,4-$(SiMe_3)_2$-2,-4-$C_2B_4H_4]_2$ (III), and *closo*-1-Ni(TMEDA)-2,4-$(SiMe_3)_2$-2,4-$C_2B_4H_4$ (IV). Colorless, prismatic, and platelike crystals of **I** and **II** and orange platelike crystals of **IV** were grown from saturated benzene solutions *in vacuo*, while the yellow prismatic crystals of **III** were sublimed *in vacuo* onto a glass surface. The crystals were all coated with an epoxy resin and mounted on a Siemens R3m/V diffractometer. The pertinent crystallographic data are summarized in Table I. The final unit cell parameters were obtained by least-squares fit of 24 accurately centered reflections measured in the ranges $16° < 2\theta < 24°$, $17° < 2\theta < 30°$, $18° < 2\theta < 29°$, and $16° < 2\theta < 29°$, and the intensity data were collected at 230 K in the ranges $3.5° \le 2\theta \le 42.0°$, $3.5° \le 2\theta \le 42.0°$, $3.5° \le 2\theta \le 44.0°$, and $3.5° \le 2\theta \le 42.0°$ for **I–IV**, respectively. Three standard reflections monitored after every 150 reflections did not show any significant change in intensity during the data collection. The data were corrected for Lorentz and polarization effects in all four cases. However, semiempirical absorption corrections (based on ψ scans) were applied with the minimum and maximum transmission factors of 0.5671 and 0.5983, and 0.7645 and 1.0000, for **III** and **IV**, respectively. The structures were solved by either direct or heavy-atom methods using the SHELXTL-Plus package.[5] Full-matrix least-squares refinements were performed and the scattering factors, with anomalous dispersion correction for Ni in the cases of **III** and **IV**, were taken from ref 6. All non-H atoms were refined anisotropically. In the structure of **I**, the methyl carbons on Si(2) were statistically disordered and, therefore, were elastically constrained during refinement. Consequently, the carbon atoms, labeled as C(10), C(11), and C(12), were placed in 46% occupancy, while the remaining occupancy was designated as C(10′), C(11′), and C(12′) atoms in Table II. Compound **I** is a dimer that possesses a center of symmetry at the midpoint of the Li(1)–Li(1a) line (symmetry operator a: $-x, 2-y, 1-z$), while **III** contains a 2-fold rotation axis that is parallel to the *b* axis and passes through the central Ni atom. Carborane cage-H atoms were located in difference Fourier maps in all structures. The cage-H's of **II** were isotropically refined. However, the methyl- and methylene-H atoms were calculated and contrained tetrahedrally. The final cycles of refinement converged at R = 0.076, 0.060, 0.033, and 0.041, R_w = 0.095, 0.064, 0.040, and 0.052, and GOF = 2.83, 1.57, 1.18, and 1.58 for **I–IV**, respectively. The final atomic coordinates are given in Table II, while selected bond lengths and bond angles are presented in Table III.

(5) Sheldrick, G. M. *Structure Determination Software Programs*; Siemens X-ray Analytical Instrument Corp.: Madison, WI, 1990.
(6) *International Tables For X-ray Crystallography*; Kynoch Press: Birmingham, U.K., 1974; Vol. IV.

Table I. Crystal Data[a] for I–IV

	I	II	III	IV
formula	$C_{32}H_{58}O_4B_8Si_4Li_4$	$C_{20}H_{54}N_4B_4Si_2Li_2$	$C_{16}H_{44}B_8Si_4Ni$	$C_{14}H_{38}N_2B_4Si_2Ni$
fw	733.4	464.0	494.1	392.6
cryst syst	monoclinic	monoclinic	orthorhombic	monoclinic
space group	$P2_1/n$	$P2_1/n$	$Pbcn$	$P2_1/n$
a, Å	11.353(5)	9.828(4)	12.409(3)	8.310(2)
b, Å	17.490(7)	22.267(7)	18.436(5)	19.657(4)
c, Å	13.273(6)	15.064(5)	12.976(3)	14.655(3)
β, deg	104.33(3)	95.87(3)	90.00	94.14(2)
V, Å^3	2551(2)	3279(2)	2969(1)	2387.6(9)
Z	2	4	4	4
D_{calcd}, g cm^{-3}	0.955	0.940	1.105	1.092
abs coeff, mm^{-1}	0.139	0.117	0.818	0.913
cryst dmns, mm	0.20 × 0.35 × 0.25	0.15 × 0.30 × 0.05	0.20 × 0.30 × 0.15	0.15 × 0.25 × 0.05
scan type	$\theta/2\theta$	$\omega/2\theta$	$\theta/2\theta$	$\omega/2\theta$
scan sp in ω; min, max	5.0, 25.0	6.0, 30.0	6.0, 30.0	6.0, 30.0
2θ range, deg	3.5–42.0	3.5–42.0	3.5–44.0	3.5–42.0
T, K	230	230	230	230
decay, %	0	0	0	0
no. of data collcd	3032	3915	2110	2916
no. of obsd reflctns, $I > 3.0\sigma(I)$	1739	2282 [$I > 2.0\sigma(I)$]	1274	1924
no. of params refined	263	305	132	208
GOF	2.83	1.57	1.18	1.58
g[c]	0.0005	0.0005	0.0005	0.0005
$\Delta\rho_{max,min}$, e/Å^3	0.30, –0.27	0.24, –0.21	0.24, –0.20	0.30, –0.37
R[b]	0.076	0.060	0.033	0.041
R_w	0.095	0.064	0.040	0.052

[a] Graphite monochromatized Mo Kα radiation, λ = 0.710 73 Å. [b] $R = \sum||F_o| - |F_c||/\sum|F_o|$, $R_w = [\sum w(F_o - F_c)^2/\sum w(F_o)^2]^{1/2}$. [c] $w = 1/[\sigma^2(F_o) + g(F_o)^2]$.

Calculations. Molecular orbital calculations were carried out on the model complexes *closo*-1-(TMEDA)Ni-2,4-$C_2B_4H_6$ (**V**) and *commo*-1,1′-Ni(2,4-$C_2B_4H_6)_2$ (**VI**) using the unparameterized Fenske–Hall method.[7] The basis functions used were those generated by the numerical Xα atomic orbital program of Herman and Skillman,[8] used in conjunction with the Xα-to-Slater program of Bursten and Fenske.[9,10] The heavy atom positions in **V** and **VI** were taken as the analogous atom positions in **IV** and **III**, respectively. The relative positions of the hydrogens were the MNDO[11] optimized ones for [*nido*-2,4-$C_2B_4H_6]^{2-}$. In the calculations a coordinate system was defined such that the C_2B_3 pentagonal face was in the xy plane, and the unique boron, B(2) in Figures 3 and 4, was on the x axis. Although this coordinate system did not take advantage of the 2-fold rotational axis in **III**, it yielded molecular orbitals that had the same basis as those used for other metallacarboranes in the pentagonal bipyramidal system.[1]

Results and Discussion

Synthesis. The reductive cage opening reaction of carbons adjacent *closo*-1,2-$(SiMe_3)_2$-1,2-$C_2B_4H_4$ with 2 equiv of lithium naphthalide in THF produced the corresponding THF-solvated carbons apart dilithium compound, *closo-exo*-5,6-[$(\mu$-H$)_2$Li(THF)](μ-THF)-1-Li-2,4-$(SiMe_3)_2$-2,4-$C_2B_4H_4$ (**I**), in almost quantitative yield (*ca.* 93%). Our preliminary report described a general methodology for the preparation of such species, and the X-ray analysis of the corresponding disodium compound showed that the compound existed as discrete dimers in which each carborane dianion was associated with an *endo*-sodium, which adopted an essentially η^5-bonding posture with respect to the C_2B_3 face, and an exopolyhedral sodium that was situated over a B_3 trigonal face formed by the apical boron and the two basal borons. Each sodium was also coordinated with sufficient THF molecules (2–3) to give a roughly tetrahedral arrangement of groups (THF's and carboranes) about the metal.[3] The structure of the dilithium compound **I**, shown in Figure 1, is similar to that of the disodium species, except that there are fewer THF molecules of solvation and there seems to be direct Li–Li interactions (the relevant distances are Li(1)–Li(1a) = 2.709 Å, Li(1)–Li(2a) = 2.889 Å, see Table III). On the other hand, when the cage opening reaction was carried out in TMEDA, the monomeric carbons apart dilithi-

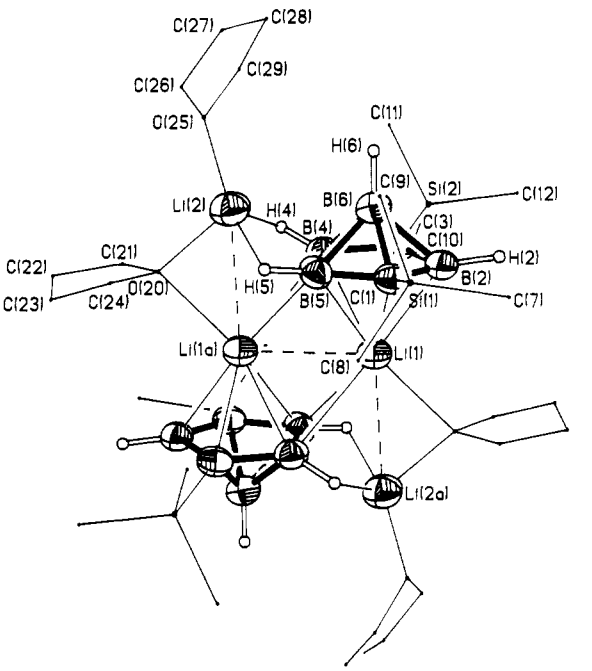

Figure 1. Perspective view of a discrete dimeric unit of *closo-exo*-5,6-[$(\mu$-H$)_2$Li(THF)](μ-THF)-1-Li-2,4-$(SiMe_3)_2$-2,4-$C_2B_4H_4$ (**I**) showing the atom numbering scheme with thermal ellipsoids drawn at the 40% probability level. The molecule possesses a symmetric center at the midpoint of Li(1)–Li(1a). The atoms of the $SiMe_3$ groups and THF molecules are drawn with circles of arbitrary radii.

(7) Hall, M. B.; Fenske, R. F. *Inorg. Chem.* **1972**, *11*, 808.
(8) Herman, F.; Skillman, S. *Atomic Structure Calculations*; Prentice-Hall: Englewood, NJ, 1963.
(9) (a) Bursten, B. E.; Fenske, R. F. *J. Chem. Phys.* **1977**, *67*, 3138. (b) Bursten, B. E.; Jensen, R. J.; Fenske, R. F. *J. Chem. Phys.* **1978**, *68*, 3320.
(10) We wish to thank Prof. M. B. Hall, Texas A&M University, for furnishing a copy of this program.

Table II. Atomic Coordinates (×10⁴) and Equivalent Isotropic Displacement Coefficients (Å² × 10³)

	x	y	z	U(eq)[b]		x	y	z	U(eq)[b]
				Compound I					
Li(1)	−383(9)	9305(6)	5236(8)	51(4)	C(12)	1899(22)	6896(6)	5705(16)	129(15)
Li(2)	2826(10)	10528(7)	6063(9)	64(5)	C(10′)[a]	1090(12)	7154(9)	4310(13)	239(21)
Si(1)	293(2)	9571(1)	8186(1)	57(1)	C(11′)[a]	3212(14)	8261(8)	4321(13)	98(9)
Si(2)	2221(2)	7840(1)	5133(2)	65(1)	C(12′)[a]	3209(15)	7309(10)	6279(9)	160(13)
C(1)	638(5)	9316(4)	6947(5)	44(3)	O(20)	2157(4)	11379(3)	5167(4)	65(2)
B(2)	738(6)	8516(5)	6492(6)	49(3)	C(21)	2655(8)	11539(6)	4317(8)	103(5)
C(3)	1456(5)	8626(4)	5647(5)	48(3)	C(22)	2754(15)	12380(11)	4256(15)	208(12)
B(4)	1722(6)	9482(4)	5491(6)	47(3)	C(23)	2156(16)	12655(9)	4970(15)	214(13)
B(5)	1204(7)	9951(4)	6365(6)	47(3)	C(24)	2054(9)	12089(6)	5656(8)	109(5)
B(6)	2048(7)	9108(5)	6765(6)	52(3)	O(25)	4488(4)	10604(4)	6749(5)	89(3)
C(7)	−461(8)	8762(5)	8687(6)	91(4)	C(26)	4864(13)	10993(9)	7677(11)	201(9)
C(8)	−753(7)	10407(4)	7974(7)	91(4)	C(27)	5527(18)	10507(13)	8395(15)	378(19)
C(9)	1703(7)	9847(5)	9182(5)	83(4)	C(28)	5720(12)	9826(10)	8001(15)	207(11)
C(10)	1621(20)	7811(11)	3670(6)	163(17)	C(29)	5269(9)	9983(7)	6809(10)	135(7)
C(11)	3919(7)	8014(11)	5474(18)	174(16)					
				Compound II					
Li(1)	5397(8)	6335(3)	2495(5)	46(3)	N(21)	6365(5)	5521(2)	2097(3)	63(2)
Li(2)	3521(9)	7966(3)	2617(5)	49(3)	N(22)	7498(5)	6602(2)	2796(4)	73(2)
Si(1)	3372(2)	6192(1)	4529(1)	54(1)	C(23)	7795(6)	5652(3)	2077(6)	107(4)
Si(2)	2239(2)	6336(1)	647(1)	47(1)	C(24)	8348(7)	6079(3)	2718(6)	111(4)
C(1)	3643(5)	6400(2)	3387(3)	39(2)	C(25)	5778(7)	5260(3)	1272(5)	111(4)
B(2)	3161(6)	6019(3)	2554(4)	37(2)	C(26)	6151(6)	5108(3)	2806(5)	92(3)
C(3)	3163(4)	6435(2)	1747(3)	35(2)	C(27)	7682(6)	7026(3)	2108(5)	108(4)
B(4)	3764(6)	7066(3)	2028(4)	39(2)	C(28)	7824(7)	6877(4)	3642(6)	140(4)
B(5)	4070(6)	7042(3)	3109(4)	40(2)	N(31)	2062(5)	8523(2)	3062(3)	61(2)
B(6)	2493(6)	6753(3)	2638(4)	42(2)	N(32)	4477(5)	8737(2)	2210(3)	55(2)
C(7)	2195(6)	5540(2)	4579(4)	84(3)	C(33)	2346(6)	9111(3)	2681(5)	85(3)
C(8)	2672(7)	6821(3)	5153(4)	98(3)	C(34)	3803(7)	9216(2)	2656(4)	86(3)
C(9)	5041(6)	5980(3)	5151(4)	99(3)	C(35)	683(6)	8355(3)	2741(4)	91(3)
C(10)	1506(7)	5572(2)	479(4)	92(3)	C(36)	2189(7)	8531(3)	4018(4)	113(4)
C(11)	3443(5)	6453(3)	−216(3)	73(2)	C(37)	5924(6)	8743(3)	2473(5)	103(3)
C(12)	830(6)	6886(3)	428(4)	85(3)	C(38)	4243(7)	8791(3)	1244(4)	91(3)
				Compound III					
Ni	0	3963(1)	7500	23(1)	B(6)	846(4)	4077(3)	5601(3)	31(2)
Si(1)	2748(1)	4670(1)	7103(1)	35(1)	C(7)	2588(4)	5574(3)	7692(3)	61(2)
Si(2)	−462(1)	2544(1)	5448(1)	38(1)	C(8)	3478(3)	4059(3)	8004(3)	55(2)
C(1)	1396(3)	4289(2)	6760(3)	25(1)	C(9)	3497(3)	4739(3)	5865(3)	53(2)
B(2)	1178(4)	3449(3)	6625(3)	30(2)	C(10)	327(4)	1748(2)	5878(4)	62(2)
C(3)	53(3)	3391(2)	6076(3)	28(1)	C(11)	−1901(3)	2405(3)	5787(4)	64(2)
B(4)	−516(4)	4131(3)	5969(3)	30(2)	C(12)	−308(5)	2673(3)	4039(4)	75(2)
B(5)	432(4)	4767(3)	6428(3)	30(2)					
				Compound IV					
Ni	1894(1)	7972(1)	5332(1)	36(1)	C(10)	1574(9)	5926(3)	3589(5)	100(3)
Si(1)	3063(2)	9088(1)	3352(1)	54(1)	C(11)	5010(8)	5870(3)	4404(4)	79(3)
Si(2)	2962(2)	6205(1)	4563(1)	54(1)	C(12)	2251(8)	5834(3)	5622(5)	84(3)
C(1)	3103(6)	8364(3)	4148(3)	36(2)	N(21)	−530(5)	7940(2)	5201(3)	53(2)
B(2)	2229(8)	7665(3)	3976(4)	39(2)	N(22)	1751(5)	8303(3)	6585(3)	52(2)
C(3)	3071(6)	7140(3)	4661(3)	38(2)	C(23)	−1045(9)	8206(5)	6067(6)	110(4)
B(4)	4168(7)	7506(3)	5390(5)	45(2)	C(24)	33(8)	8172(5)	6771(5)	124(5)
B(5)	4169(7)	8341(3)	5048(4)	39(2)	C(25)	−1240(7)	8366(3)	4462(5)	93(3)
B(6)	4361(8)	7684(3)	4222(4)	42(2)	C(26)	−1121(6)	7245(3)	5056(4)	68(3)
C(7)	1874(13)	8936(4)	2307(5)	185(6)	C(27)	2114(11)	9013(4)	6681(5)	116(4)
C(8)	2358(11)	9839(3)	3922(6)	117(4)	C(28)	2723(8)	7934(4)	7278(4)	84(3)
C(9)	5128(9)	9279(4)	3050(6)	129(4)					

[a] C(10′), C(11′), and C(12′) of structure I, 54% of occupancy, are disordered with C(10), C(11), and C(12), 46%, respectively. [b] Equivalent isotropic U defined as one-third of the trace of the orthogonalized U_{ij} tensor.

acarborane, *closo-exo*-5,6-[(μ-H)$_2$Li(TMEDA)]-1-Li(TMEDA)-2,4-(SiMe$_3$)$_2$-2,4-$C_2B_4H_4$ (**II**), was isolated in 90% yield. The solvent dependence of the cage opening process shows that a strongly coordinating solvent, such as TMEDA, restricts the dimer formation and hence yields simple monomer entities, consisting of one *endo*- and one *exo*-polyhedrally oriented group 1 metal. This same general structural pattern was found in the carbons adjacent isomers. Indeed, the structure of **II** is very similar to that of the corresponding carbons adjacent dilithium complex.[1]

The reactivities of the dilithium compounds, **I** and **II**, toward $NiCl_2$ are quite different. The reaction of **I** (the THF-solvated dilithium compound) with $NiCl_2$, in a 1:1 molar ratio, produces the carbons apart *commo*-1,1′-Ni-[2,4-(SiMe$_3$)$_2$-2,4-$C_2B_4H_4$]$_2$ (**III**) and elemental nickel (Ni^0) in almost equal quantities. Although the exact mechanism of this reaction is not known, it is not unreasonable to assume that the reaction involves the initial formation of a *closo*-nickelacarborane, of the type 1-Ni-2,4-(SiMe$_3$)$_2$-2,4-$C_2B_4H_4$ (THF molecules are not included), as an intermediate, which rapidly undergoes a disproportionation reaction to yield the Ni(IV) sandwich complex, **III**, and Ni^0. On the other hand, the TMEDA-complexed species, *closo*-1-Ni(TMEDA)-2,4-(SiMe$_3$)$_2$-2,4-$C_2B_4H_4$ (**IV**), was obtained as the major product from the similar reaction of $NiCl_2$ with the TMEDA-solvated dilithium compound, **II**. The trapping, or stabilization, of the *closo*-nickel-

Table III. Selected Bond Lengths (Å) and Bond Angles (deg)

Bond Lengths

Compound I

Li(1)–Li(1a)[a]	2.709(22)	Li(1)–Li(2a)	2.889(14)	Li(2)–O(25)	1.882(11)	C(1)–B(2)	1.540(10)
Li(1)–Cnt(1)[b]	1.891	Li(1)–C(1)	2.275(11)	C(1)–B(5)	1.578(10)	C(1)–B(6)	1.717(10)
Li(1)–B(2)	2.289(12)	Li(1)–C(3)	2.344(12)	B(2)–C(3)	1.556(11)	B(2)–B(6)	1.774(11)
Li(1)–B(4)	2.349(12)	Li(1)–B(5)	2.327(12)	C(3)–B(4)	1.552(10)	C(3)–B(6)	1.692(9)
L(1)–B(4a)	2.648(13)	Li(1)–B(5a)	2.467(13)	B(4)–B(5)	1.646(12)	B(4)–B(6)	1.763(11)
Li(1)–O(20a)	2.288(11)	Li(2)–B(4)	2.238(14)	B(5)–B(6)	1.767(11)	Si(1)–C(1)	1.839(7)
Li(2)–B(5)	2.222(15)	Li(2)–O(20)	1.938(12)	Si(2)–C(3)	1.845(7)		

Compound II

Li(1)–Cnt(2)	1.908	Li(1)–C(1)	2.295(9)	B(2)–B(6)	1.771(8)	C(3)–B(4)	1.566(7)
Li(1)–B(2)	2.318(10)	Li(1)–C(3)	2.374(9)	C(3)–B(6)	1.708(7)	B(4)–B(5)	1.626(8)
Li(1)–B(4)	2.344(9)	Li(1)–B(5)	2.299(10)	B(4)–B(6)	1.767(8)	B(5)–B(6)	1.760(8)
Li(1)–N(21)	2.160(9)	Li(1)–N(22)	2.151(9)	Si(1)–C(1)	1.827(5)	Si(2)–C(3)	1.820(4)
Li(2)–B(4)	2.215(10)	Li(2)–B(5)	2.234(9)	B(2)–H(2)	1.11(4)	B(4)–H(4)	1.12(3)
Li(2)–N(31)	2.059(10)	Li(2)–N(32)	2.078(9)	Li(2)–H(4)	1.92(3)	B(5)–H(5)	1.07(3)
C(1)–B(2)	1.548(7)	C(1)–B(5)	1.560(7)	Li(2)–H(5)	1.96(3)	B(6)–H(6)	1.18(4)
C(1)–B(6)	1.705(7)	B(2)–C(3)	1.528(7)				

Compound III

Ni–Cnt(3)	1.597	Ni–C(1)	2.070(4)	B(2)–B(6)	1.810(7)	C(3)–B(4)	1.541(6)
Ni–B(2)	2.080(5)	Ni–C(3)	2.128(4)	C(3)–B(6)	1.717(6)	B(4)–B(5)	1.765(7)
Ni–B(4)	2.110(5)	Ni–B(5)	2.102(5)	B(4)–B(6)	1.759(7)	B(5)–B(6)	1.741(7)
C(1)–B(2)	1.583(6)	C(1)–B(5)	1.546(6)	Si(1)–C(1)	1.873(4)	Si(2)–C(3)	1.875(4)
C(1)–B(6)	1.698(6)	B(2)–C(3)	1.571(6)				

Compound IV

Ni–Cnt(4)	1.662	Ni–C(1)	2.207(5)	C(1)–B(6)	1.696(8)	B(2)–C(3)	1.568(8)
Ni–B(2)	2.115(6)	Ni–C(3)	2.178(5)	B(2)–B(6)	1.782(9)	C(3)–B(4)	1.533(8)
Ni–B(4)	2.097(6)	Ni–B(5)	2.094(6)	C(3)–B(6)	1.676(8)	B(4)–B(5)	1.716(9)
Ni–N(21)	2.011(4)	Ni–N(22)	1.959(5)	B(4)–B(6)	1.766(9)	B(5)–B(6)	1.785(9)
C(1)–B(2)	1.567(8)	C(1)–B(5)	1.536(7)	Si(1)–C(1)	1.838(5)	Si(2)–C(3)	1.845(5)

Bond Angles

Compound I

Cnt(1)–Li(1)–Li(1a)	87.9	Cnt(1)–Li(1)–Li(2a)	174.8	B(2)–C(3)–B(6)	66.0(5)	B(4)–C(3)–B(6)	65.7(6)
Cnt(1)–Li(1)–O(20a)	134.8	Cnt(1)–Li(1)–B(4a)	133.3	Li(1)–B(4)–Li(2)	128.3(5)	C(3)–B(4)–B(5)	105.7(6)
Cnt(1)–Li(1)–B(5a)	136.3	Li(1a)–Li(1)–Li(2a)	95.0(5)	C(3)–B(4)–B(6)	61.0(4)	B(5)–B(4)–B(6)	62.3(5)
Li(1a)–Li(1)–B(4a)	52.0(4)	Li(2a)–Li(1)–B(4a)	47.4(3)	Li(1)–B(4)–Li(1a)	65.3(5)	Li(2)–B(4)–Li(1a)	72.0(4)
Li(1a)–Li(1)–O(20a)	136.9(6)	Li(2a)–Li(1)–O(20a)	42.0(3)	Li(1)–B(5)–Li(2)	130.3(6)	C(1)–B(5)–B(4)	104.8(6)
B(4a)–Li(1)–O(20a)	86.7(4)	B(5a)–Li(1)–O(20a)	87.4(4)	C(1)–B(5)–C(6)	61.5(4)	B(4)–B(5)–B(6)	62.1(5)
B(4)–Li(2)–O(20)	108.7(5)	B(5)–Li(2)–O(20)	104.2(5)	Li(1)–B(5)–Li(1a)	68.7(5)	Li(2)–B(5)–Li(1a)	75.9(4)
B(4)–Li(2)–O(25)	129.0(7)	B(5)–Li(2)–O(25)	136.1(7)	C(1)–B(6)–B(2)	52.3(4)	C(1)–B(6)–C(3)	92.9(4)
O(20)–Li(2)–O(25)	115.6(7)	B(4)–Li(2)–Li(1a)	60.6(4)	B(2)–B(6)–C(3)	53.3(4)	C(1)–B(6)–B(4)	94.4(5)
B(5)–Li(2)–Li(1a)	55.9(4)	O(20)–Li(2)–Li(1a)	52.2(3)	B(2)–B(6)–B(4)	93.3(5)	C(3)–B(6)–B(4)	53.3(4)
O(25)–Li(2)–Li(1a)	167.6(7)	B(2)–C(1)–B(5)	117.7(6)	C(1)–B(6)–B(5)	53.9(4)	B(2)–B(6)–B(5)	93.6(5)
B(2)–C(1)–B(6)	65.7(5)	B(5)–C(1)–B(6)	64.7(5)	C(3)–B(6)–B(5)	95.0(5)	B(4)–B(6)–B(5)	55.6(4)
C(1)–B(2)–C(3)	105.9(6)	C(1)–B(2)–B(6)	62.0(4)	Li(2)–O(20)–Li(1a)	85.8(5)		
C(3)–B(2)–B(6)	60.7(4)	B(2)–C(3)–B(4)	111.7(6)				

Compound II

N(21)–Li(1)–Cnt(2)	135.5	N(22)–Li(1)–Cnt(2)	143.0	C(1)–B(5)–B(4)	105.7(4)	C(1)–B(5)–B(6)	61.5(3)
N(21)–Li(1)–N(22)	81.4(3)	N(31)–Li(2)–N(32)	87.2(3)	B(4)–B(5)–B(6)	62.8(3)	C(1)–B(6)–B(2)	52.8(3)
B(2)–C(1)–B(5)	110.7(4)	B(2)–C(1)–B(6)	65.7(3)	C(1)–B(6)–C(3)	92.6(3)	B(2)–B(6)–C(3)	52.1(3)
B(5)–C(1)–B(6)	65.0(3)	C(1)–B(2)–C(3)	106.7(4)	C(1)–B(6)–B(4)	94.0(4)	B(2)–B(6)–B(4)	92.3(4)
C(1)–B(2)–B(6)	61.4(3)	C(3)–B(2)–B(6)	61.8(3)	C(3)–B(6)–B(4)	53.5(3)	C(1)–B(6)–B(5)	53.5(3)
B(2)–C(3)–B(4)	111.1(4)	B(2)–C(3)–B(6)	66.1(3)	B(2)–B(6)–B(5)	92.8(4)	C(3)–B(6)–B(5)	94.3(4)
B(4)–C(3)–B(6)	65.2(3)	Li(1)–B(4)–Li(2)	127.4(4)	B(4)–B(6)–B(5)	54.9(3)	Li(2)–H(4)–B(4)	89(2)
C(3)–B(4)–B(5)	105.6(4)	C(3)–B(4)–B(6)	61.3(3)	Li(2)–H(5)–B(5)	90(2)		
B(5)–B(4)–B(6)	62.3(3)	Li(1)–B(5)–Li(2)	128.7(4)				

Compound III

Cnt(2)–Ni–Cnt(3b)	174.4	B(2)–C(1)–B(5)	113.2(3)	C(1)–B(5)–B(6)	61.9(3)	B(4)–B(5)–B(6)	60.2(3)
B(2)–C(1)–B(6)	66.9(3)	B(5)–C(1)–B(6)	64.7(3)	C(1)–B(6)–B(2)	53.5(2)	C(1)–B(6)–C(3)	94.7(3)
C(1)–B(2)–C(3)	105.5(3)	C(1)–B(2)–B(6)	59.6(3)	B(2)–B(6)–C(3)	52.8(2)	C(1)–B(6)–B(4)	97.6(3)
C(3)–B(2)–B(6)	60.5(3)	B(2)–C(3)–B(4)	112.9(3)	B(2)–B(6)–B(4)	93.2(3)	C(3)–B(6)–B(4)	52.6(2)
B(2)–C(3)–B(6)	66.7(3)	B(4)–C(3)–B(6)	65.1(3)	C(1)–B(6)–B(5)	53.4(2)	B(2)–B(6)–B(5)	94.7(3)
C(3)–B(4)–B(5)	104.6(3)	C(3)–B(4)–B(6)	62.3(3)	C(3)–B(6)–B(5)	98.5(3)	B(4)–B(6)–B(5)	60.5(3)
B(5)–B(4)–B(6)	59.2(3)	C(1)–B(5)–B(4)	103.4(3)				

Compound IV

N(21)–Ni–Cnt(4)	134.6	N(22)–Ni–Cnt(4)	136.9	B(5)–B(4)–B(6)	61.7(4)	C(1)–B(5)–B(4)	105.5(4)
N(21)–Ni–N(22)	88.4(2)	B(2)–C(1)–B(5)	110.1(4)	C(1)–B(5)–B(6)	60.8(3)	B(4)–B(5)–B(6)	60.6(4)
B(2)–C(1)–B(6)	66.1(4)	B(5)–C(1)–B(6)	66.8(4)	C(1)–B(6)–B(2)	53.5(3)	C(1)–B(6)–C(3)	96.9(4)
C(1)–B(2)–C(3)	107.2(4)	C(1)–B(2)–B(6)	60.4(3)	B(2)–B(6)–C(3)	53.8(3)	C(1)–B(6)–B(4)	96.9(4)
C(3)–B(2)–B(6)	59.6(3)	B(2)–C(3)–B(4)	110.6(4)	B(2)–B(6)–B(4)	91.9(4)	C(3)–B(6)–B(4)	52.8(3)
B(2)–C(3)–B(6)	66.6(4)	B(4)–C(3)–B(6)	66.6(4)	C(1)–B(6)–B(5)	52.3(3)	B(2)–B(6)–B(5)	90.9(4)
C(3)–B(4)–B(5)	105.0(4)	C(3)–B(4)–B(6)	60.6(4)	C(3)–B(6)–B(5)	96.3(4)	B(4)–B(6)–B(5)	57.8(4)

[a] Symmetry operator a: $-x, 2-y, -z$ in structure I. Symmetry operator b: $-x, y, {}^3/_2 - z$ in structure III. [b] Cnt(1) stands for the centroid of C(1), B(2), ..., B(5) in structure I; Cnt(2) in II; ...; and Cnt(4) in IV.

Scheme I

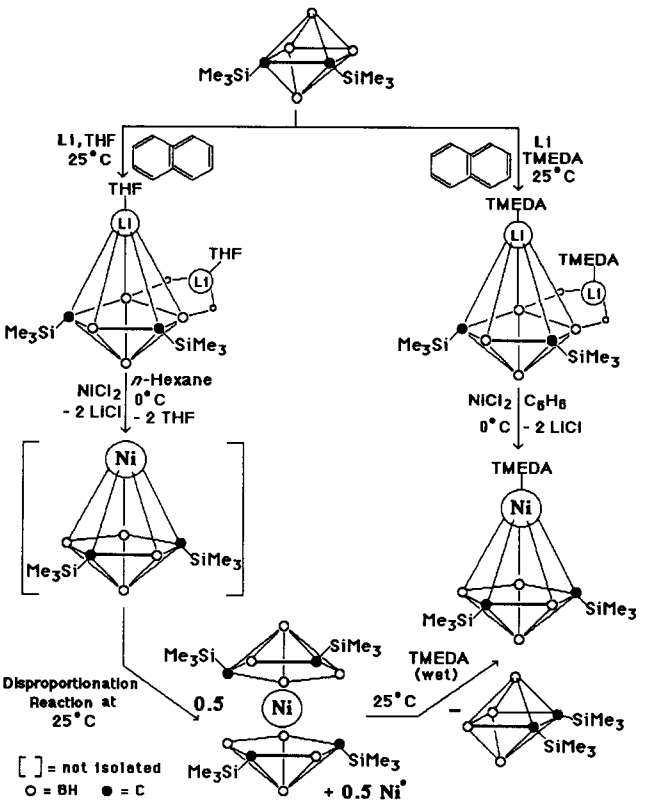

acarborane by TMEDA is consistent with the proposed initial formation of a half-sandwich intermediate complex in the disproportion reaction that produced the bis(carboranyl)nickel sandwich complex, **III**. Schematic representations for the preparations of the dilithium precursors, **I** and **II**, and their subsequent conversions to nickelacarborane complexes, **III** and **IV**, are shown in Scheme I. Irrespective of the exact mechanism for the production of **III**, the results clearly indicate that a strong base, such as TMEDA, prevents the disproportionation reaction of the *closo*-nickelacarborane by stabilizing the nickel atom. However, other factors are also important in determining whether the reaction of the dilithium compound with a metal halide will lead to a redox reaction or a simple ligand exchange reaction. For example, the reactions of $NiCl_2$ with either the analogous unsolvated, THF-solvated, or TMEDA-solvated carbons adjacent dilithiacarboranes underwent instantaneous redox reactions to produce elemental nickel (Ni^0) and the *closo*-1,2-dicarbahexaborane(6) derivative.[1] MNDO-SCF calculations[11] on the free [*nido*-2,3-$(SiMe_3)_2$-2,3-$C_2B_4H_4]^{2-}$ and [*nido*-2,4-$(SiMe_3)_2$-2,4-$C_2B_4H_4]^{2-}$ dianions show that the latter is 28.8 kcal/mol more stable than the former. This increased thermodynamic stability of the carbons apart isomers over their carbons adjacent analogues has been recognized for some time and is of importance in dictating the course of metal–carborane reactions.[12]

The redox chemistry of the nickelacarboranes is somewhat complex and demonstrates not only the ability of the TMEDA to stabilize the half-sandwich Ni(II) complex but also the stabilization of high oxidation states in metals that are involved in full-sandwiched carborane compounds. The stabilization of metals in unusually high oxidation states when they are sandwiched between *nido*-carborane dianions has been observed in both the pentagonal bipyramidal and icosahedral systems.[13-16] Nickel(II) does not oxidize the carbons apart *nido*-carborane dianion as it does the carbons adjacent isomer; in the presence of TMEDA, simple ligation of the Ni(II) occurs giving the TMEDA stabilized half-sandwich nickelacarborane. However, without TMEDA, the reaction of $NiCl_2$ with the *nido*-carborane dianion results in a disproportionation of the nickel, giving Ni^0 and the Ni^{IV} sandwich compound, in very high yields (the 37% yield quoted in the Experimental Section respresents 74% of the maximum yield expected under the reaction conditions used). When the nickel(IV) sandwich compound, **III**, reacts with TMEDA, a reductive displacement of a carborane takes place in which one of the bonding electron pairs of the leaving carborane is retained by the nickel, giving the TMEDA-complexed Ni(II) half-sandwich complex, **IV**, and the *closo*-carborane; this reaction leads to 86% yield. It is of interest to note that the *closo*-carborane formed is the precursor 1,2-isomer, rather than the reportedly more thermodynamically stable 1,6-isomer.[17] At this point, it is not known whether the formation of *closo*-1,2-$(SiMe_3)_2$-1,2-$C_2B_4H_4$ by the two electron oxidation of either the respective carbons apart or carbons adjacent *nido*-carborane dianions is kinetically controlled or if the $SiMe_3$ substituents on the cage carbons materially affect the relative stabilities of the *closo*-isomers. This is currently under investigation in our laboratories. It should also be noted that, unlike the metallacarboranes in which the metal is sandwiched by mixed π-C_5H_5 (or other arene) and C_2B_4-carborane ligands, the nickelacarboranes do not seem to undergo so-called "decapitation" reactions with wet TMEDA at room temperature.[18] Instead, in the nickel system, the TMEDA attacks the metal rather than the apical BH unit.

Spectra. Compounds **I–IV** were all characterized by ^1H, ^{11}B, and ^{13}C pulse Fourier transform NMR and IR spectroscopy. In addition, the ^7Li NMR spectra were obtained for both **I** and **II**, and the high-resolution electron impact (HREI) mass spectra were obtained for **III** and **IV** (Experimental Section).

The ^1H and ^{13}C NMR spectra and IR spectra of the dilithium compounds **I** and **II** are all consistent with the formulations of the compounds given in the Experimental Section and with their solid state structures (Figures 1 and 2) and are quite similar to those of the corresponding carbons adjacent isomers.[1] The ^7Li NMR spectrum of **II** is almost identical to that of its carbons adjacent isomer and, for the reasons outlined for that isomer,[1] the resonance at δ –1.60 is assigned to the *exo*-cage lithium, while the resonance at δ –6.08 is assigned to the *endo*-cage lithium.

(11) Version 5.01 of the MOPAC Package. See: Stewart, J. J. P. *QCPE Bull.* **1983**, *3*, 43.

(12) (a) Grimes, R. N. In *Comprehensive Organometallic Chemistry*; Wilkinson, G., Stone, F. G. A., Abel, E. W., Eds.; Pergamon: Oxford, U.K., 1982; Vol 1, Chapter 5.5 (see also references therein). (b) Sneddon, L. G.; Beer, D. C.; Grimes, R. N. *J. Am. Chem. Soc.* **1973**, *95*, 6623. (c) Miller, V. R.; Grimes, R. N. *J. Am. Chem. Soc.* **1973**, *95*, 2830. (d) Miller, V. R.; Sneddon, L. G.; Beer, D. C.; Grimes, R. N. *J. Am. Chem. Soc.* **1974**, *96*, 3090. (e) Grimes, R. N.; Beer, D. C.; Sneddon, L. G.; Miller, V. R.; Weiss, R. *Inorg. Chem.* **1974**, *13*, 1138. (f) Barker, G. K.; Green, M.; Stone, F. G. A.; Welch, A. J. *J. Chem. Soc., Dalton Trans.* **1980**, 1186.

(13) (a) Warren, L. F., Jr.; Hawthorne, M. F. *J. Am. Chem. Soc.* **1968**, *18*, 4823. (b) Warren, L. F., Jr.; Hawthorne, M. F. *J. Am. Chem. Soc.* **1967**, *89*, 470.

(14) St. Clair, D.; Zalkin, A.; Templeton, D. H. *J. Am. Chem. Soc.* **1970**, *92*, 1173.

(15) Oki, A. R.; Zhang, H.; Maguire, J. A.; Hosmane, N. S.; Ro, H.; Hatfield, W. E.; Moscherosch, M.; Kaim, W. *Organometallics* **1992**, *11*, 4202.

(16) Jia, L.; Zhang, H.; Hosmane, N. S. *Organometallics* **1992**, *11*, 2957.

(17) Williams, R. E. *Chem. Rev.* **1992**, *92*, 177.

(18) Grimes, R. N. *Chem. Rev.* **1992**, *92*, 251.

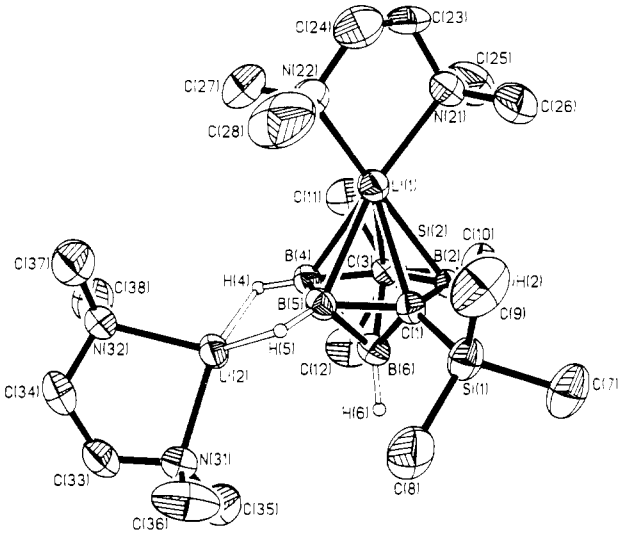

Figure 2. Perspective view of the monomeric *closo-exo*-5,6-[(μ-H)$_2$Li(TMEDA)]-1-Li(TMEDA)-2,4-(SiMe$_3$)$_2$-2,4-$C_2B_4H_4$ (**II**) showing the atom numbering scheme with thermal ellipsoids drawn at the 40% probability level. The methyl and methylene H's are omitted for clarity.

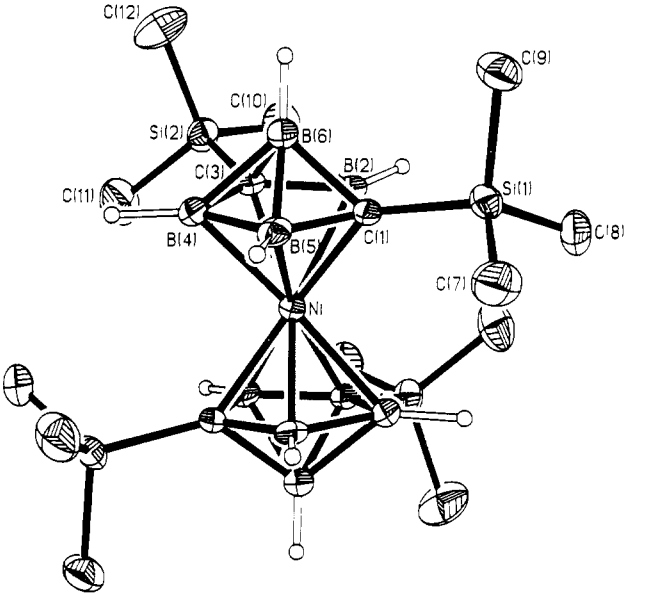

Figure 3. Perspective view of the "carbons apart" Ni(IV) complex *commo*-1,1'-Ni[2,4-(SiMe$_3$)$_2$-2,4-$C_2B_4H_4$]$_2$ (**III**) with thermal ellipsoids drawn at the 40% probability level and showing the atom numbering scheme. The molecule contains a 2-fold rotation axis that is parallel to the *b* axis and is passing through the central Ni atom. The silylmethyl H's are omitted for clarity.

Compound **I** also shows two ^{7}Li NMR resonances, the resonance at δ 1.42 relaxes faster than the other and is near the standard chemical shift value of 0 ppm of the purely ionic $LiNO_3$; therefore, it can be assigned to the *exo*-polyhedral lithium and the very broad resonance at δ 2.73 to that of the *endo*-cage lithium. The chemical shifts in the ^{7}Li NMR spectra of both the lithium atoms in **I** are shifted downfield when compared to those of **II**, indicating that the lithium atoms in **I** are more deshielded. At this point it is not readily apparent what specific interactions lead to this increased deshielding, both the difference in number and type of solvating molecules and, if the structure shown in Figure 1 persists in solution, the dimeric nature of the complex and the direct Li···Li contacts (2.71–2.89 Å) may all make contributions. The increased broadness of the *exo*-cage lithiums in the ^{1}H-coupled ^{7}Li NMR spectra of **I** and **II** could be due to the presence of the Li–H–B bridges that are found in their crystal structures (see Table III).

The ^{11}B NMR spectra of **I** and **II** are more diagnostic of the relative positions of the cage carbons than are the other spectroscopic results. The ^{11}B NMR spectra of both the carbons apart and the carbons adjacent isomers are similar in that all show resonances in the δ −40 to −50 region due to the apical borons, with the basal boron resonance occurring in the δ 0–20 range. However, in compounds **I** and **II** the ^{11}B NMR resonances of the unique boron, that is, the boron lying in the pseudomirror plane of the C_2B_4 cage, are shifted downfield (δ 16.25 in **I** and 18.02 in **II**) when compared with those of the corresponding carbons adjacent isomers (δ 2.36–3.18).[1] This is not surprising in view of the fact that in **I** and **II** the unique borons are bonded to two electronegative carbon atoms, while in the carbons adjacent isomers the carbons are bonded to the other two basal borons. The resulting 1:2:1 peak area distribution in the ^{11}B NMR spectra of **I** and **II** distinguishes them from their corresponding carbons adjacent isomers, in which the peak area ratios are in 2:1:1 patterns.[1]

The ^{11}B NMR spectra of the nickelacarboranes, **III** and **IV**, show apical boron resonances of δ 5.92 and −10.81, respectively, which are significantly shifted downfield from the analogous resonances in the precursor lithium compounds (δ −42 to −49). Such shifts of the apical boron resonances have been observed when the carbons adjacent carboranes bond with metals and have been interpreted in terms of the withdrawal of electron density from the carborane on metal complexation.[19] The much smaller downfield shift seen in **IV** indicates that a significant amount of electron density is transferred back to the cage borons after complexation of the nickelacarborane with the electron-rich TMEDA base. The ^{11}B NMR spectrum of **III** does not show any differentiation of the basal borons but consists of only a single broad peak at δ 18.7. This could be due to the accidental overlap of the basal boron resonances or some fluxionality in the complex that prevents the differentiation of the basal boron atoms by NMR. On the other hand, the half-sandwich complex, **IV**, shows two basal boron resonances with relative intensities of 2:1 at δ 3.72 and −3.74, for boron atoms B(4,5) and B(2), respectively (see Figure 4 for the atom numbering system). The higher downfield shift of the basal boron resonance in **III**, when compared to **IV**, is consistent with that found for their apical boron resonances and is probably due to the same type of interactions. The two separate resonances of the SiMe$_3$ groups in both the ^{1}H and ^{13}C NMR spectra of **III**, in addition to two nonequivalent ^{13}C resonances of the cage carbons, is a clear indication that the two C_2B_4 cages are not symmetrically arranged about the Ni center in solution. This is consistent with the staggered arrangement of the cage carbons as found in the solid state structure of **III**, shown in Figures 3 and 8.

The high resolution electron impact mass spectra (HREI) and the isotope patterns of both the *commo*-nickelacarborane, **III**, and *closo*-nickelacarborane, **IV**, are consistent with their molecular formulas whose exact

(19) (a) Hosmane, N. S.; Maguire, J. A. *Adv. Organomet. Chem.* **1990**, *30*, 99. (b) Maguire, J. A.; Fagner, J. S.; Siriwardane, U.; Banewicz, J. J.; Hosmane, N. S. *Struct. Chem.* **1990**, *1*, 583. (c) Maguire, J. A.; Ford, G. P.; Hosmane, N. S. *Inorg. Chem.* **1988**, *27*, 3354.

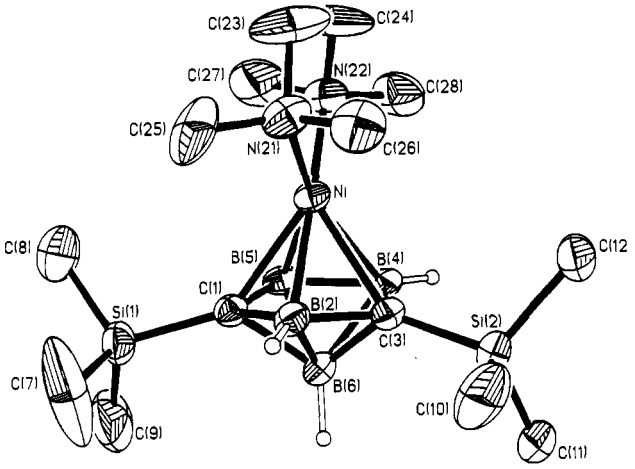

Figure 4. Perspective view of the "carbons apart" Ni(II) complex *closo*-1-Ni(TMEDA)-2,4-$(SiMe_3)_2$-2,4-$C_2B_4H_4$ (**IV**) with thermal ellipsoids drawn at the 40% probability level and showing the atom numbering scheme. The methyl and methylene H's are omitted for clarity.

masses give excellent fits between experimental and theoretical *m/z* values (see Experimental Section).

Crystal Structure Analyses of the Dimeric *closo-exo*-5,6-[(μ-H)$_2$Li(THF)](μ-THF)-1-Li-2,4-$(SiMe_3)_2$-2,4-$C_2B_4H_4$ (I), the Monomeric *closo-exo*-5,6-[(μ-H)$_2$Li(TMEDA)]-1-Li(TMEDA)-2,4-$(SiMe_3)_2$-2,4-$C_2B_4H_4$ (II), *commo*-1,1′-Ni[2,4-$(SiMe_3)_2$-2,4-$C_2B_4H_4$]$_2$ (III), and *closo*-1-Ni(TMEDA)-2,4-$(SiMe_3)_2$-2,4-$C_2B_4H_4$ (IV) and Molecular Orbital Analysis. The crystal structures of the lithium compounds, **I** and **II**, are shown in Figures 1 and 2, and some pertinent bond distances and bond angles are listed in Table III. The THF-solvated lithium compound, **I**, exists in the solid as a fairly tight ion cluster consisting of two $Li_2C_2B_4$ units with a center of symmetry halfway between Li(1) and Li(1a). The lithiums are not equivalent in that Li(1) and Li(1a) occupy capping positions above the C_2B_3 open carborane faces, giving a pentagonal bipyramidal lithiacarborane structure, while Li(2) and Li(2a) are in *exo*-polyhedral positions between the two adjacent borons of the C_2B_3 face of the carborane. The short Li(2)–B(4) and Li(2)–B(5) interatomic distances, 2.238 and 2.222 Å, respectively, indicate that the Li atoms bond to their respective hydrogens, giving B–H–Li bridges; the absorptions due to these B–H–Li bridges are also evident in the solution IR spectrum of **I** (see Experimental Section). The IR spectral results, coupled with the nonequivalent Li's in the ^{7}Li NMR of **I**, indicate that $Li_2C_2B_4$ units, very similar to the one shown in Figure 1, also exist in solutions of low dielectric constant solvents, such as benzene. The results neither indicate nor disallow more extensive ion clustering in solution. In **I** there are also four THF molecules of crystallization lining the outside of the cluster and solvating the lithium atoms. Considering the placement of THF molecules and the carboranes, each lithium could be considered to be four-coordinated; however, this coordination is very uneven and there are direct Li···Li interactions in the interior of the cluster. As discussed earlier, the unusual chemical shifts in the ^{7}Li NMR spectrum of **I** could also be taken as an indication that extensive dimerization also occurs in solution. When the Li^+ ions are coordinated by a strong bulky base, such as TMEDA, to form **II**, the dimeric structure is broken and individual dilithium species occupy the unit cell (see Figure 2). The structure of **II** is almost identical with that of its corresponding carbons adjacent isomer; there are two (TMEDA)Li groups, one occupying a capping position above the C_2B_3 carborane face and the other in a bridging position between the two adjacent basal borons. The solution IR and ^{7}Li NMR spectra are all consistent with this structure, indicating that Figure 2 also depicts the structure of the solution species of **II**. The TMEDA on the capping lithium is aligned in the pseudomirror plane of the $Li_2C_2B_4$ cage, this alignment is the one that would give the smallest steric interaction between the $SiMe_3$ moiety and the TMEDA molecule.

The structure of the TMEDA stabilized half-sandwich nickelacarborane, **IV**, is quite similar to that of the corresponding lithiacarborane, **II**, in that in both complexes the metal is centered over the open C_2B_3 carborane. However, as discussed above, the ^{11}B NMR spectrum of **IV** gives a clear indication of strong metal–carborane bonding. Most of the structural studies of the metallacarboranes in the pentagonal bipyramidal system have involved complexes of the carbons adjacent carborane dianions.[12a,18–20] However, Stone and co-workers have reported the structure of the carbons apart Pt(II) complex, *closo*-1,1-$(Et_3P)_2$-1,2,4-$PtC_2B_4H_6$, along with its carbons adjacent isomer *closo*-1,1-$(Et_3P)_2$-2,3-Me_2-1,2,3-$PtC_2B_4H_4$.[12f] The structure of the carbons adjacent complex showed that the Et_3P–Pt–PEt_3 plane was oriented perpendicular to the mirror plane of the PtC_2B_4 cage and that the Pt was slipped toward the unique boron. There were two crystallographically independent molecules in the unit cell of the carbons apart platinacarborane isomer, one in which the Pt was symmetrically bonded to the carborane face and the Et_3P–Pt–PEt_3 plane was contained in the C_2B_4 mirror plane, and another in which the Et_3P–Pt–PEt_3 plane was rotated out of the C_2B_4 mirror plane by about 23° and the Pt was displaced slightly away from one of the cage carbons. However, neither of the carbons apart platinacarboranes show a slippage of the metal along the mirror plane of the carborane, as was found in the carbons adjacent isomer. A qualitative understanding of some of the factors governing the relationship between ligand orientation and metal slippage in these d^8 metallacarboranes can be understood by referring to Figures 5–7. Figure 5 shows the molecular orbital correlation diagram for the model compound 1-(TMEDA)Ni-2,4-$C_2B_4H_6$ (**V**) in terms of its $NiC_2B_4H_6$ and TMEDA fragments; also included are sketches of some of the more important $NiC_2B_4H_6$ fragment orbitals in terms of their input atomic orbitals. Supplementary Table S-4 gives the compositions of the filled MO's of **V**, as well as some of its lower energy virtual MO's. This molecular orbital analysis shows that the main bonding interactions in the $NiC_2B_4H_6$ fragment are between the metal's $3d_{xz}$ and $3d_{yz}$ orbitals and a set of symmetry matched π-type carborane orbitals. Fragment orbitals NC14a′ and NC12a″ are the bonding pairs resulting from these interactions, while NC19a′ and NC18a″ are the respective antibonding orbitals. Fragment orbitals NC17a′, NC16a′, and NC15a″ are heavily localized on the metal, having 71% $3d_{x^2-y^2}$, 90% $3d_{z^2}$, and 89% $3d_{xy}$ character, respectively, and their energies do not differ greatly from those of the input 3d metal orbitals. The electron count in the fragment is such that NC18a″ is its HOMO and NC19a′ is its LUMO. Figure 6 shows plots of the energies of fragment orbitals NC19a′ through NC15a″ as a function of Δ, which is defined as the lateral

(20) Weiss, R.; Bryan, R. F. *Acta Crystallogr., Sect. B* **1977**, *33*, 589.

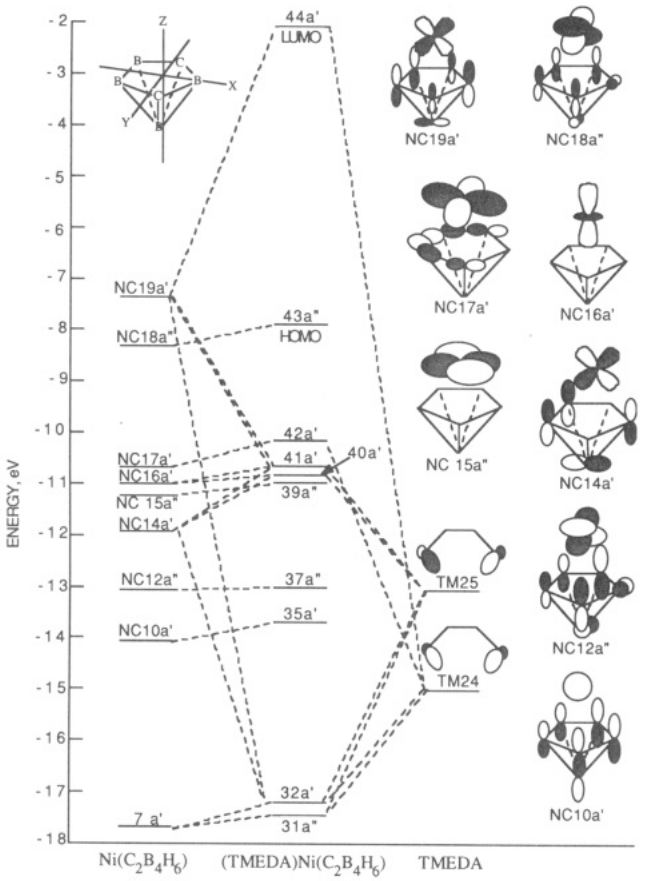

Figure 5. Molecular orbital correlation diagram for *closo*-1-Ni(TMEDA)-2,4-$C_2B_4H_6$ (**V**) in terms of its Ni($C_2B_4H_6$) and TMEDA fragments.

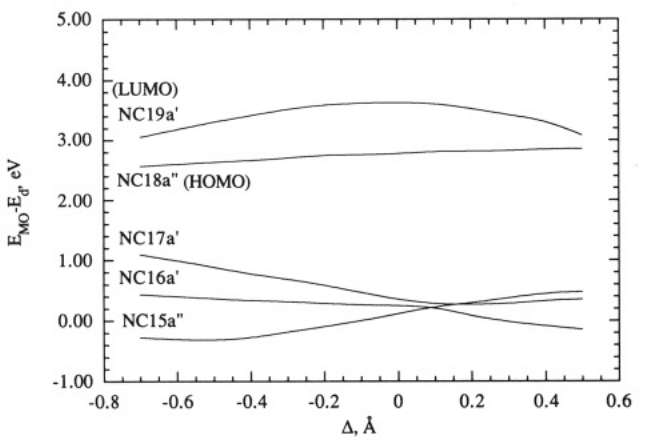

Figure 6. Plot of $E_{MO} - E_d$ for several $NiC_2B_4H_6$ orbitals as a function of Δ. E_{MO} = energy of the fragment orbital, E_d = energy of the input metal d orbitals, and Δ is the displacement in the mirror plane of the metal away from a symmetric position.

displacement, in angstroms, of the metal in the carborane's mirror plane from the normal drawn from the C_2B_3 face to the apical boron [B(6) in Figure 4]; a positive value of Δ indicates a slippage toward the unique boron [B(2) in Figure 4].[21] As can be seen from Figure 6, the energy changes in orbitals NC15a″ through NC17a′ are opposing and tend to cancel one another, while the energy of fragment orbital NC18a″ increases slowly with Δ. On the other hand, fragment orbital NC19a′ is greatly stabilized

(21) For reference, the values of Δ for the C_2B_3 atoms are B(4,5) = −1.07, C(1,3) = 0.41, B(2) = 1.32.

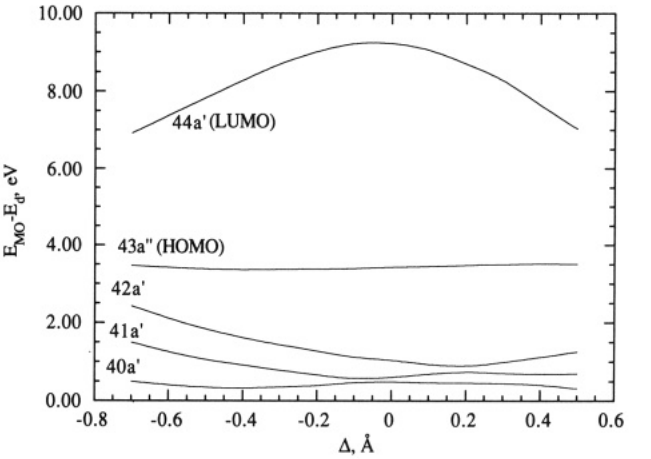

Figure 7. Plot of $E_{MO} - E_d$ for several (TMEDA)$NiC_2B_4H_6$ molecular orbitals as a function of Δ. E_{MO} = energy of the molecular orbital, E_d = energy of the input metal d orbitals, and Δ is the displacement in the mirror plane of the metal away from a symmetric position.

on slippage of the metal. Depending on the relative orientation of the TMEDA, fragment orbitals NC19a′ and NC18a″ are the ones that would be expected to interact most strongly with the base's lone pair orbitals. If the nitrogens of the TMEDA were oriented in the mirror plane of the nickelacarborane, as is found experimentally, then $NiC_2B_4H_6$ fragment orbital NC19a′ would interact strongly, while NC18a″ would be orthogonal; a perpendicular orientation of the TMEDA would give the reverse. The nickelacarborane–TMEDA orbital interactions give rise to the correlation diagram shown in Figure 5. Figure 7 shows the energies of some of the resulting MO's of **V** as a function of Δ. As can be seen from this plot, the occupied MO's of **V** experience very little net stabilization on slippage, and a symmetrically bound Ni would be expected. On the other hand, if the base nitrogens were oriented perpendicular to the metallacarborane mirror plane, NC19a′ would be orthogonal to the lone pair base orbitals, the positions of MO43a″ and 44a′ would be reversed, and a slip distortion of the metal would be expected. Since the calculations show a reasonable energy separation between the HOMO and LUMO nickelacarborane fragment, the TMEDA molecule should orient to maximize interaction with NC19a′, that is, lie in the mirror plane of the complex. Molecular orbital calculations were carried out at the hypothetical carbons adjacent nickelacarborane fragment, 1,2,3-$NiC_2B_4H_6$, with the Ni occupying a position above the C_2B_3 carborane face equivalent to that found in **IV**. The calculation produced an energy level sequence similar to that found for the carbons apart fragment shown in Figure 5, with the exception that the orbitals equivalent to NC19a′ and NC18a″ were essentially degenerate, differing in energy by 0.01 eV. Therefore, either one could just as easily interact with a set of lone pair base orbitals and no base orientation preference could be predicted by the calculations. Although the above arguments are qualitative and consider only effects arising from fragment overlap, they do provide a rationale for the structure of **IV** and the distortion-base orientation pattern found in the platinacarboranes reported by Stone and co-workers.[12f] Therefore, for the d^8 metallacarboranes with heavy atom formulations of the type $L_2MC_2B_4$ (L = Lewis base coordinated to the metal), one would expect slippage of the metal only when the base ligands, L, are oriented

perpendicular to the mirror plane of the complex. This was the same general conclusion reached by Mingos and co-workers, starting from a slightly different point of view, for the 11-vertex bis(trialkylphosphine)platinacarboranes.[22]

Steric interaction also seems to favor an orientation of the TMEDA base in the mirror plane of the carbons apart metallacarboranes. Semiempirical MNDO[11] molecular orbital calculations on the model ionic complex 1-(TMEDA)M-2,4-$C_2B_4H_6$ (M = a purely ionic dipositive cation), with the same nearest neighbor distances as in **V**, showed that TMEDA–carborane repulsion increased as the TMEDA was rotated out of the mirror plane to a perpendicular orientation. The presence of the $SiMe_3$ substituents on the cage carbons in **IV** would only tend to increase the effects of this TMEDA–carborane repulsion.

The structure of the neutral full-sandwich nickelacarborane, **III**, given in Figure 3, shows that the nickel is symmetrically bonded to two parallel C_2B_3 carborane faces; the pertinent bond distances are Ni–B(4) = 2.110 Å, Ni–B(5) = 2.102 Å, Ni–C(1) = 2.070 Å, Ni–C(3) = 2.128 Å, and Ni–B(2) = 2.080 Å (see Table III). These distances are similar to those found in the icosahedral Ni^{IV}–carborane sandwich complexes; the Ni–B(basal), Ni–B(unique), and Ni–C(cage) distances in $Ni^{IV}(1,2\text{-}C_2B_9H_{11})_2$ are 2.10, 2.12, and 2.07 Å, respectively, and in the racemic (3,4′)-$[(CH_3)_2C_2B_9H_9]_2Ni$ complex the analogous distances are 2.07, 2.10, and 2.19 Å, respectively.[14,23] These distances are not too different from the values of 2.108, 2.160, and 2.146 Å for the respective Ni–B(basal), Ni–B(unique), and Ni–C(cage) distances in the $[Ni^{III}(1,2\text{-}C_2B_9H_{11})_2]^-$ ion.[24] Crystal structures of both the carbons adjacent and carbons apart icosahedral Ni^{II} sandwich complexes, $[3,3'\text{-}Ni^{II}(1,2\text{-}C_2B_9H_{11})_2]^{2-}$ and $[3,3'\text{-}Ni^{II}(1,7\text{-}C_2B_9H_{11})_2]^{2-}$, have also been reported.[25] In the carbons apart isomer the C_2B_3 faces are not planar, and several supposedly equivalent facial-atom bonds are unequal in length.[25b] However, with the exception of one unusually long Ni–ring-atom bond distance, the others are within ±0.04 Å of an average value of 2.14 Å, which is only slightly larger than the distances found in **III**. In the carbons adjacent isomer, the nickel is slip distorted toward the unique boron; this slip distortion is typical of the more electron rich transition metal metallacarborane sandwich complexes (d^8 and greater).[25a] This insensitivity of the metal–carborane bond distances to the oxidation state of the metal is a characteristic of both the icosahedral and pentagonal bipyramidal metallacarborane sandwich complexes.[15,23–25] One other interesting structural feature of **III** is that, although the two carborane pentagonal faces are essentially parallel, the carboranes are twisted such that the C_2B_3 faces are almost eclipsed, and the cage carbons are not symmetrically located about the metal; Figure 8 shows the relative positions of these C_2B_3 faces. As can be seen in this figure, the faces are twisted such that the pseudomirror planes of the C_2B_4 cages intersect at a dihedral angle of 81.8°.

Figure 9 shows the molecular orbital correlation diagram for the model compound 1,1′-$Ni^{IV}(2,4\text{-}C_2B_4H_6)_2$ (**VI**) in terms of its $NiC_2B_4H_6$ and $C_2B_4H_6$ fragments. The

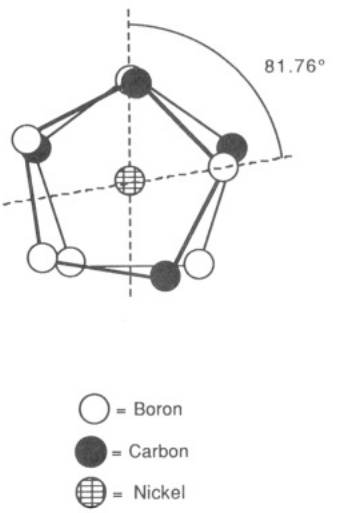

Figure 8. View of the relative positions of the C_2B_3 carborane faces in **III** as viewed down one of the apical boron–nickel axes. For clarity, only the basal atoms are shown.

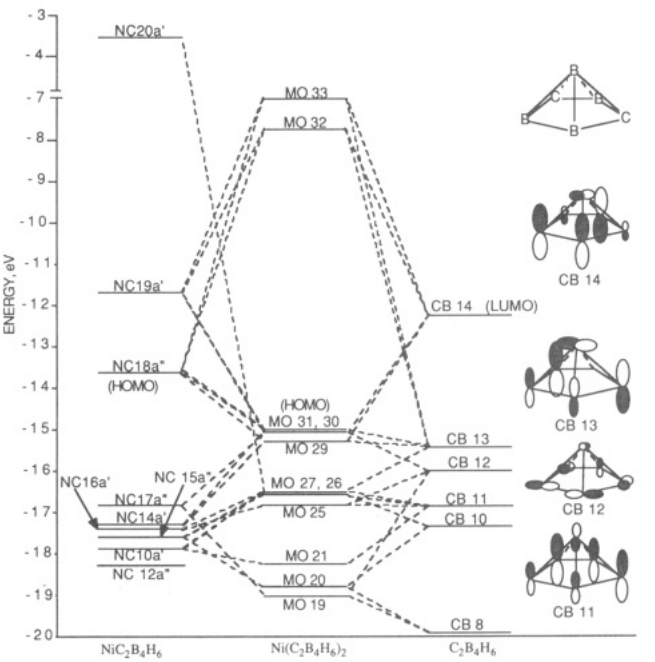

Figure 9. Molecular orbital correlation diagram for *commo*-1,1′-$Ni(2,4\text{-}C_2B_4H_6)_2$ (**VI**) in terms of its $Ni(C_2B_4H_6)$ and $C_2B_4H_6$ fragments.

compositions of the molecular orbitals of **VI** are given in Supplementary Table S-5. Since the $Ni(C_2B_4H_6)_2$ complex has no plane of symmetry, the notations a′ and a″ have no meaning for the complex but will still be retained when referring to the $NiC_2B_4H_6$ fragment. Figure 9 also shows sketches of the important carborane fragment orbitals, while the metal containing fragments orbitals are sketched in Figure 5. The HOMO is MO 31 so that, at least in a formal way, the metal's d^6 valence electrons begin filling MO 29. In **VI**, MO 31 contains 14.8% Ni character (7.6% 3d and 7.2% 4p) and gives rise to some of the stronger interfragment bonding interactions. Molecular orbital 30, whose energy is essentially the same as that of MO 31, is localized more on the carboranes (79%) than on the metal but contains essentially no carborane π character. Molecular orbital 29 is similar to MO 31 in that it is composed of about equal parts Ni(3d) [9.6%] and Ni(4p) [7.0%] characters. From the molecular orbital energy sequence

(22) (a) Mingos, D. M. P. *J. Chem. Soc., Dalton Trans.* **1977**, 602. (b) Mingos, D. M. P.; Forsyth, M. I.; Welch, A. J. *J. Chem. Soc., Dalton Trans.* **1978**, 1363. (c) Mingos, D. M. P.; Forsyth, M. I.; Welch, A. J. *J. Chem. Soc., Chem. Commun.* **1977**, 605.
(23) Churchill, M. R.; Gold, K. *J. Am. Chem. Soc.* **1970**, *92*, 1180.
(24) Hansen, F. V.; Hazell, R. G.; Hyatt, C.; Stucky, G. D. *Acta Chem. Scand.* **1973**, *27*, 1210.
(25) (a) Wing, R. M. *J. Am. Chem. Soc.* **1968**, *90*, 4828. (b) Wing, R. M. *J. Am. Chem. Soc.* **1970**, *92*, 1187.

shown in Figure 9 it is apparent that a d^6 metal configuration would be extremely stable, and the unusual +4 oxidation state of the Ni found in **III** is understandable. The energy level sequence shown in Figure 9 has much in common with those found for the carbons adjacent sandwich complexes, such as $[1,1'\text{-}Cr(2,3\text{-}C_2B_4H_6)_2]^n$ (n = 0, −1), which is probably typical for the early transition metal complexes and for the cyclopentadienide and icosahedral transition metal sandwich complexes.[15,26,27] All show that the major bonding interactions are between ligand π-type orbitals and the metal $3d_{xz}$ and $3d_{yz}$ orbitals and that the metal d^n electrons are distributed in a set of five MO's having roughly the same general energy pattern as shown in Figure 9, that is, two closely spaced high energy MO's arising from antibonding carborane–metal(d_{xz}, d_{yz}) interactions and, at much lower energies, three MO's corresponding to MO's 31 through 29. The main difference lies in the nature of the three lower energy orbitals. In the earlier transition metal sandwich complexes, these MO's are highly metal centered orbitals that are essentialy the metal's d_{z^2}, $d_{x^2-y^2}$, and d_{xy} orbitals, while with the later transition metals the orbitals are more carborane centered and the metal participation is distributed almost equally between the metal's 3d and 4p orbitals (see above).[26]

Increased metal 4p bonding may also contribute to the lower symmetry of **III** when compared to *commo*-metallacarboranes of the earlier transition metal complexes. Molecular orbital calculations on **VI** and its C_{2v} (carbons eclipsed) and C_{2h} (carbon trans) isomers show a HOMO/LUMO gap larger in **VI** (7.27 eV) than in either the C_{2v} (5.04 eV) or the C_{2h} (4.82 eV) isomers. Analysis of the results shows that the difference is due mainly to a lowering of the energy of the HOMO in **VI** (Mo 31 in Figure 9). In **VI**, MO 31 contains about equal parts 3d and 4p character (see above), while in the other two isomers the orbital has essentially no 3d contribution. Therefore, the increased participation of the lower energy 3d orbitals in the HOMO on going to a lower symmetry conformation should tend to stabilize the complex. Models also show that the experimental carborane configuration results in a slightly greater separation of the $SiMe_3$ groups than would be found in either of the more symmetric complex geometries. Although these arguments help rationalize the experimental structure of **III**, it should be emphasized that they are *ad hoc*, and at the present level of analysis, it is impossible to tell unequivocally whether the experimental configuration, shown in Figure 3, is the result of internal bonding preferences or of crystal packing forces operating on a shallow potential energy surface. The fact that the ^{11}B NMR spectrum of **III** shows only a single broad resonance for the facial borons could indicate fluxionality in the complex; however, the ^{13}C and ^1H NMR spectra are consistent with a more rigid structure.

This initial report on the half-sandwich and full-sandwich complexes of the carbons apart carboranes indicates that these ligands should produce a wider and more varied range of metallacarboranes than found for the corresponding carbons adjacent carborane system. The ligating abilities of the two carborane systems seem to be comparable; however, the increased stability of the carbons apart *nido*-cages toward oxidative cage closure should greatly increase the range of metals that will coordinate with these carboranes rather than oxidize them. An extensive study of the ligation chemistry of these carboranes is currently underway in our laboratories.

Acknowledgment. This work was supported by grants from the National Science Foundation (CHE-9100048), the Robert A. Welch Foundation (N-1016), and the donors of the Petroleum Research Fund, administered by the American Chemical Society. Mass spectral determinations were made at the Midwest Center for Mass Spectrometry with partial support by the National Science Foundation, Biology Division (Grant No. DIR9017262). We thank Dr. R. E. Williams and his associates at the Loker Hydrocarbon Research Institute, University of Southern California for many valuable suggestions concerning the cage-opening reactions.

Supplementary Material Available: Tables of selected bond lengths and bond angles (Table S-1), anisotropic displacement parameters (Table S-2), and H atom coordinates and isotropic displacement coefficients (Table S-3) for **I**, **II**, **III**, and **IV**, tables of orbital compositions for **V** (Table S-4) and **VI** (Table S-5), and figures of the atom numbering system for **V** and **VI** (23 pages). Ordering information is given on any current masthead page.

OM930253J

(26) Mingos, D. M. P.; Forsyth, M. I. *J. Organomet. Chem.* **1978**, *146*, C37.

(27) Haaland, A. *Acc. Chem. Res.* **1979**, *12*, 415.